Nitric oxide-inducible Fe-S cluster biogenesis enables *Mycobacterium tuberculosis* to persist in mice

Kushi Anand[1], Ashutosh Tripathi[1], Kaustubh Shukla[2], Nitish Malhotra[3], Anilkumar Jamithireddy[4], Rajiv Kumar Jha[5], Susmit Narayan Chaudhury[3], Raju S Rajmani[1], Arati Ramesh[3], Valakunja Nagaraja[5], Balasubramanian Gopal[4], Ganesh Nagaraju[2] , Aswin Sai Narain Seshayee[3], and Amit Singh*[1, 5]

[1]Centre for Infectious Disease Research, Indian Institute of Science, Bangalore 560012, India. [2]Department of Biochemistry, Indian Institute of Science, Bangalore 560012, India. [3]National Centre for Biological Science, Bangalore 560065, India. [4]Molecular Biophysics Unit, Indian Institute of Science, Bangalore 560012, India. [5]Department of Microbiology and Cell Biology, Indian Institute of Science, Bangalore 560012, India.

***Correspondence**

Amit Singh, Ph.D
Associate Professor
Wellcome Trust-India Alliance Senior Fellow
Department of Microbiology and Cell Biology (MCBL)
Centre for Infectious Disease and Research (CIDR)
Indian Institute of Science (IISc)
Bangalore-12
Ph:+91 8022932604
asingh@iisc.ac.in

Abstract

Host-inducible nitric oxide (NO) suppresses *Mycobacterium tuberculosis* (*Mtb*) without eradicating it. Mechanisms underlying the persistence of residual bacteria in a hostile host environment are not known. Since NO damages Fe-S clusters of essential enzymes, the mechanism used to repair Fe-S clusters could help *Mtb* persist in host tissues. Here, we show that *Mtb* utilizes the *suf* operon (*Rv1460-Rv1466*) for Fe-S cluster biogenesis to persist under NO stress. Further, transcriptional repressor SufR (*Rv1460*) senses NO through its 4Fe-4S cluster to directly regulate Suf-meditated Fe-S cluster biogenesis. We discovered that NO inflicted irreversible damage upon Fe-S clusters to exhaust respiratory reserves and redox buffering capacity of *MtbΔsufR*. Importantly, *MtbΔsufR* failed to recover from a NO-induced non-growing state and displayed persistence defect inside immune-activated macrophages and murine lungs in a NO-dependent manner. Data suggest that SufR is a sensor of NO that supports persistence by reprogramming Fe-S cluster metabolism and bioenergetics of *Mtb*.

Introduction

About 90% of an estimated 2 billion people infected with *Mycobacterium tuberculosis* (*Mtb*) remain asymptomatic for tuberculosis (TB). This indicates that the host immune system effectively suppresses the pathogen's replication without eradicating the pathogen. The ability of the host to produce nitric oxide (NO) by an inducible nitric oxide synthase (iNOS) is known to modulate host immunity (1) and microbial physiology (2), thereby controlling diverse infections (3,4) including TB (5). Upon infection with *Mtb*, lesional macrophages in humans and macaques express functional iNOS (6,7), and exhaled breath of TB patient contains NO (8). Importantly, iNOS activity seems to control TB in humans (9,10). Mechanistically, NO inhibits respiration and arrests growth of *Mtb* (2). The bacterial mechanisms responsible for sensing NO and mobilizing adaptation programs are poorly understood.

Previously published models suggest that *Mtb* exploits a three-component system, DosR/S/T, to induce transcriptional changes, growth arrest, and a switch from aerobic to anaerobic respiration to enhance survival under NO stress (11,12). However, the NO-mediated activation of DosR regulon is transient(13) and other gases, such as carbon monoxide (CO) and oxygen (O_2-limitation), similarly activate the DosR pathway (14,15). Therefore, the underlying regulatory mechanism that specifically coordinates changes in metabolism, growth, and respiration of *Mtb* in response to NO remains unknown.

82 NO is believed to affect bioenergetics by targeting heme, Fe-S clusters,
83 mycothiol, and protein thiols in *Mtb* (16). In this context, a recent study
84 demonstrated active degradation of several iron-sulfur cluster (Fe-S) proteins
85 coordinating respiration, central metabolism, and amino acid biosynthesis in
86 NO-treated *Mtb* (13). In addition, a seven-gene operon, the Suf system
87 (*Rv1460-Rv1466*) that is likely involved in Fe-S cluster biogenesis (17),
88 showed prolonged, elevated expression in response to NO (13). Other targets
89 of NO, such as haemoglobins, cytochrome C oxidase, and thiol proteins,
90 remained unaffected (13), supporting the significance of Fe-S cluster
91 homeostasis in remedying NO stress in *Mtb*. Moreover, NO modulates the
92 regulatory activity of two redox sensors, WhiB3 and WhiB1, by targeting their
93 Fe-S clusters (18-20). Since the reaction of NO with Fe-S clusters generates
94 a lethal dinitrosyl-iron dithiol complex (DNIC) (21), active degradation and
95 calibrated regeneration of Fe-S clusters via the *suf* operon represents a
96 potential adaptive defense against NO. Despite these reports, how *Mtb*
97 senses the need for Fe-S cluster biogenesis in response to NO and the nature
98 of the underlying regulatory mechanisms remains uncharacterized. Filling this
99 knowledge gap is crucial to understanding the molecular underpinning of
100 persistence by this human pathogen.
101
102 In the present work, we performed transcriptomics, Fe-S enzymatic
103 assays, bioenergetics flux analysis, and redox measurements to characterize
104 the response of *Mtb* towards NO. We performed a comprehensive
105 biochemical and genetic investigation of an Fe-S cluster containing
106 transcription factor SufR (Rv1460) and established that SufR-mediated

107 regulation of Fe-S cluster biogenesis organizes the bacterial response to NO.
108 Finally, we confirmed the requirement of SufR in promoting persistence of *Mtb*
109 in response to NO in mice.

110

111 **Results**

112 **NO modulates the expression of Fe-S cluster pathways in *Mtb***
113
114 We performed transcriptomics of *Mtb* treated for 4 h with 0.5 mM of the
115 NO donor diethylenetriamine-nitric oxide (DETA-NO) by sequencing RNA
116 (RNA-seq). *Mtb* treated with 0.5 mM DETA-NO retained viability, but growth
117 was arrested (Figure 1-figure supplement 1). We identified significant changes
118 in the expression of 903 genes (fold change ≥ 2; FDR ≤ 0.05) (Supplementary
119 file 1A). Our RNA-seq data recapitulated the central themes of the NO-
120 responsive transcriptome of *Mtb*, with induction of the DosR, IdeR, Zur, and
121 CsoR regulons, and with reduced expression of RNA and protein biosynthesis
122 pathways (Figure 1-figure supplement 2 and Supplementary file 1A) (13).
123 Since NO and its congeners target lipids, DNA, and redox metabolism (22),
124 genes involved in redox homeostasis, lipid biosynthesis, and DNA repair were
125 induced (Figure 1-figure supplement 2 and Supplementary file 1A).

126

127 Since Fe-S cluster proteins are the most susceptible targets of NO
128 (23), we examined the expression of 76 genes encoding the Fe-S cluster
129 proteome of *Mtb* (Supplementary file 1B). We discovered altered expression
130 of 35 genes, 23 being up-regulated and 12 down-regulated in response to NO
131 (fold change ≥ 1.5; FDR ≤ 0.05; Figure 1 and Supplementary file 1B). Genes
132 encoding Fe-S enzymes involved in central metabolism (*acn*, *prsA*, and *udgA*)

133 and primary respiration (*nuo* operon) were down-regulated, whereas genes
134 mediating alternate respiration (*narH*, *sirA, fdxA, hycP, and fdxC*) (24),
135 alternate carbon catabolism (*korAB*, *frdB*) (25), and redox metabolism (*rubA-*
136 *B*, *cysH*, and *nadA-B*) (26-28) were induced by NO (Figure 1; Supplementary
137 file 1B). NO also induces *thiC*, which encodes a Fe-S cluster-containing
138 enzyme that generates thiamin and thiamin-dependent branched chain keto-
139 acid dehydrogenase complex (BCKADH) (Figure 1). Catabolism of branched
140 chain amino acids (BCAAs) by BCKADH generates acetyl-CoA and propionyl-
141 CoA (29), which fuel the glyoxylate cycle, methyl citrate cycle, and
142 gluconeogenesis (30). Consistent with this, NO induces the expression of
143 genes coordinating BCAAs biogenesis, glyoxylate/methyl-citrate cycles
144 (isocitrate lyase [*icl1*]), and gluconeogenesis (PEP-carboxykinase [*pckA*]) in
145 *Mtb* (Figure 1; Supplementary file 1A).
146
147 The strong reactivity of NO toward the heme iron of primary
148 cytochrome oxidase is thought to arrest respiration (2). We found that NO
149 does not affect the expression of primary terminal oxidase (cytochrome bc1-
150 aa3 complex; *qcrABC*) in *Mtb* (Figure 1). However, the expression of alternate
151 respiratory complexes (*e.g.,* NADH dehydrogenase type II [*ndh*] and
152 cytochrome BD oxidase [*cydABCD*]) (Figure 1) (31) was induced. Genes of
153 Fe-S cluster enzymes producing cofactors for respiratory quinones
154 (isoprenoid; *lytB2*, *gcpE*) (32) and nitrate reductase (molybdopterin; *moaA2*)
155 (32) were up-regulated by NO (Figure 1). Expression of transcription factors
156 containing NO-sensitive Fe-S clusters (*e.g., whiB1, whiB2, and whiB3)* was
157 induced (18,20,33) (Figure 1). Up-regulation of the Fe-S cluster transcriptome

158 indicates an increased demand for Fe-S cluster biogenesis. In agreement,
159 expression of the *suf* operon (*sufRBDCSUT*; Rv1461-Rv1466) was stimulated
160 15 to 25-fold by NO (Figure 1). Also, NO induces the cysteine biosynthetic
161 machinery that supplies sulfur for Fe-S cluster biogenesis (Figure 1). In
162 contrast, genes coordinating biosynthesis of Fe-binding heme (*hemZ*) and
163 encoding Fe-storage proteins (bacterioferretin; *bfrA-B*) were down-regulated
164 (Figure 1). These observations, along with strong induction of the *ideR*-
165 mediated iron starvation response, suggest that *Mtb* faces Fe scarcity under
166 NO stress and manages it by prioritizing the assembly of [Fe-S] clusters.
167
168 **NO modulates activity of Fe-S cluster enzyme, bioenergetics, and redox**
169 **potential of *Mtb***
170 Altered expression of the Fe-S pathways involved in metabolism and
171 respiration by NO indicates that NO might modulate these processes in *Mtb*.
172 To investigate this idea, we evaluated the activity of a 4Fe-4S-containing
173 enzyme aconitase (Acn), which functions as a critical gatekeeper of the TCA
174 cycle, and shows sensitivity to NO due to a solvent-exposed Fe atom (34). A
175 gradual decrease in Acn activity over time was observed in *Mtb* exposed to
176 0.5 mM of DETA-NO, indicating Fe-S cluster damage. At 12 h post-exposure,
177 DETA-NO triggered a 40% reduction in Acn activity without decreasing its
178 abundance (Figure 2A). Importantly, re-culturing DETA-NO-treated *Mtb* in a
179 DETA-NO-free medium significantly restored Acn activity, indicating efficient
180 mobilization of Fe-S cluster regeneration machinery (Figure 2A).
181

182 Fe-S enzymes coordinate carbon catabolism and oxidative
183 phosphorylation (OXHPHOS) (35). Therefore, we exploited Seahorse XF Flux
184 technology to analyze the influence of NO on oxygen consumption rate (OCR)
185 and extracellular acidification rate (ECAR), which are measurable readouts of
186 OXPHOS and glycolysis, respectively (36). To quantify the basal and
187 maximum rates of OCR and ECAR, we cultured *Mtb* in 7H9-glucose in an XF
188 microchamber, then exposed it to DETA-NO, and finally to the uncoupler
189 carbonyl cyanide m-chlorophenyl hydrazine (CCCP) (Figure 2B-C). Addition
190 of CCCP stimulates respiration to the maximal capacity manageable by *Mtb*.
191 The difference between basal and CCCP-induced OCR provides an estimate
192 of the spare respiratory capacity available for sustaining stress-mediated
193 bioenergetics (*e.g.,* RNI and ROI) (37). Under normal growing conditions, *Mtb*
194 displays a basal OCR of 20±0.14 pmoles/min, which increases to 85±11.7
195 pmoles/min in response to uncoupling stress by CCCP (Figure 2B). Similarly,
196 basal ECAR increases from 4.5±0.48 mpH/min to 25±4.4 mpH/min in
197 response to CCCP (Figure 2C). These data indicate that *Mtb* functions at
198 submaximal OXPHOS (~ 25%) and glycolytic (~ 20%) capacities under
199 normal growing conditions. As seen with the uncoupler CCCP, pretreatment
200 with DETA-NO also increased basal OCR in a dose-dependent manner
201 (Figure 2B). Also, DETA-NO pretreatment progressively reduces the ability of
202 *Mtb* to increase OCR or ECAR in response to CCCP (Figure 2B and 2C). As a
203 result, DETA-NO significantly decreased spare respiratory capacity in a dose-
204 dependent manner (Figure 2D), indicating that *Mtb* mobilizes its reserved
205 respiratory capacity to sustain bioenergetics in response to NO. Our data

206 indicate that NO depolarizes the cytoplasmic membrane and activates
207 respiratory reserves of *Mtb*.
208
209 Lastly, we asked whether NO perturbs redox homeostasis in *Mtb*. We
210 used a genetic biosensor (Mrx1-roGFP2) to measure the redox potential of a
211 physiologically relevant antioxidant, mycothiol (MSH), as a proxy for the
212 cytoplasmic redox potential (E_{MSH}) of *Mtb* (38). Any change in redox
213 physiology can be easily quantified by ratiometric measurements of emission
214 at 510 nm after excitation at 405 and 488 nm (38). In response to an oxidant
215 or a reductant, the biosensor ratio showed a rapid increase or decrease,
216 respectively (38). *Mtb* expressing Mrx1-roGFP2 was treated with 0.25 mM,
217 0.5 mM, and 1 mM DETA-NO, and the biosensor ratio was measured. NO
218 exposure induces an insignificant increase in the Mrx1-roGFP2 ratio,
219 indicating that *Mtb* robustly maintains cytoplasmic E_{MSH} in response to NO
220 (Figure 2E). Using a ROS-sensitive fluorescent dye CellROX, we confirmed
221 that NO induces a negligible increase in oxidative stress (Figure 2F). Overall,
222 the data indicate that NO-induced growth arrest is linked to modulation of
223 cumulative respiratory and metabolic capacities of *Mtb*.
224

225 **SufR regulates the *suf* operon and the DosR regulon in response to NO**

226 Our gene expression and biochemical data indicate that Fe-S cluster
227 homeostasis is likely to be important for *Mtb's* response towards NO. To
228 examine this possibility, we investigated the role of *Mtb* SufR, which is a
229 putative regulator of the *suf* operon involved in Fe-S cluster biogenesis (39).
230 The *suf* operon, including *sufR*, showed a maximal and a long-lasting

231 induction in response to NO (13). Except for *sufR*, other genes of the *suf*
232 operon are essential (17). Therefore, we utilized previously reported
233 *MtbΔsufR* and *sufR*-complemented (*sufR-Comp*) strains (40) and performed
234 RNA-Seq in response to NO. As with wt *Mtb*, 0.5 mM DETA-NO arrested the
235 growth of *MtbΔsufR* and *sufR-Comp* without affecting viability (Figure 3-figure
236 supplement 1). Similar to wt *Mtb*, NO similarly affected the expression of the
237 *ideR*, *zurR*, and *csoR/ricR* regulons, carbon metabolism, protein biosynthesis,
238 and respiratory enzymes in *MtbΔsufR* (Figure 3-figure supplement 2,
239 Supplementary file 1C). A direct comparison of *MtbΔsufR* with wt *Mtb* after
240 DETA-NO treatment revealed differential regulation of 67 genes (fold change
241 ≥ 1.5; FDR ≤0.05) (Figure 3 and Supplementary file 1D). Several genes of the
242 DosR regulon showed hyper-induction (≥1.5-fold; FDR ≤0.05) in *MtbΔsufR* as
243 compared to wt *Mtb* or *sufR-Comp* under NO stress (Figure 3). More
244 importantly, NO-specific induction of the *suf* operon was absent in *MtbΔsufR*
245 (Figure 3). Because SufR is a putative repressor of the *suf* operon (39), the
246 diminished expression of the *suf* operon in *MtbΔsufR* was unexpected. One
247 possibility is that by removing 345 bp internal to the *sufR* ORF (+308 to +653
248 bp) for construction of *MtbΔsufR,* we might have interrupted the NO-inducible
249 transcription of the remaining *suf* genes (*Rv1461-Rv1466*) in *MtbΔsufR*
250 (Figure 3-figure supplement 3A). However, these genes remained basally
251 expressed due to an alternate transcription start site (TSS2) upstream of
252 Rv1461 (*sufB*) (Figure 3-figure supplement 3A). Consistent with this, the
253 aberrant transcript originated from the primary TSS (TSS1) containing the
254 undeleted region of the *sufR* (+1 to +307 bp) remains induced in NO treated
255 *MtbΔsufR* (Figure 3-figure supplement 3A-B). As expected, the integration of

256 a native copy of *sufR* alone in the genome of *sufR-Comp* only restored the
257 expression of *sufR* in response to NO whereas rest of the operon remained
258 uninduced (Figure 3).

259

260 While the *suf* operon was not induced, the expression of pathways
261 requiring Fe-S clusters remained induced in NO-treated *MtbΔsufR* (Figure 3).
262 Thus, we anticipate that the heightened demand for Fe-S clusters under NO
263 stress is unlikely to be satisfied in *MtbΔsufR*. Lastly, genes encoding surface
264 antigens (*mpt70*, *mpt83*, and *fbpc*), PE-PGRS family, and redox-sensitive
265 transcription factors (*oxyS* and *Rv3334*) (41,42) were also down regulated in
266 NO-treated *MtbΔsufR* (Figure 3 and Supplementary file 1D). We also found
267 that the expression of nearly 50% of genes showing differential regulation in
268 *MtbΔsufR* was restored to approximately wt *Mtb* levels in the *sufR-Comp*
269 strain under NO stress (Figure 3 and Supplementary file 1D). Since the *suf*
270 operon remained repressed in *sufR-Comp*, the partial complementation could
271 be due to impaired activity of other transcription factors (*e.g.,* WhiB1 and
272 WhiB3) that require Fe-S clusters to regulate gene expression in response to
273 NO (18,43). Altogether, the data indicate that SufR adjusts the expression of
274 the Suf Fe-S cluster assembly system and the Dos regulon upon NO stress.

275

276 **SufR is required to maintain Fe-S cluster homeostasis, bioenergetic**
277 **reserves, and redox potential in response to NO**

278 Transcriptional data indicate altered Fe-S cluster homeostasis in
279 *MtbΔsufR*. We directly tested this idea by measuring the enzymatic activity of

280 Acn (a Fe-S enzyme) in *MtbΔsufR* under NO stress (Figure 4A). Compared to
281 wt *Mtb*, a similar decrease in Acn activity was observed in *MtbΔsufR* under
282 NO stress (Figure 4A). However, and in contrast to wt *Mtb*, reactivation of Acn
283 upon removal of NO stress was absent in *MtbΔsufR* (Figure 4A). Data
284 suggest that defective induction of the *suf* operon impairs regeneration of NO-
285 damaged Fe-S clusters in *MtbΔsufR*. As expected, *sufR-Comp* which lacks
286 induction of the *suf* operon in response to NO, did not reinstate Acn activity
287 (Figure 4-figure supplement 1).

288

289 Next, we measured OCR, ECAR, and SRC of *MtbΔsufR* in response to
290 NO as described earlier. Under normal growing conditions, *MtbΔsufR* utilizes
291 ~ 35% of its maximal respiratory capacity, which is more than *Mtb* (~ 25%)
292 (Figure 4B). Moreover, while 1 mM of DETA-NO was required to increase
293 basal OCR of wt *Mtb*, 0.25 mM was sufficient for *MtbΔsufR* (Figure 4B). This
294 suggests that *MtbΔsufR* is more sensitive to membrane depolarization by NO.
295 We also found that spare respiratory capacity of *MtbΔsufR* was significantly
296 lower than wt *Mtb* under normal culture conditions and upon exposure to 0.25
297 mM of DETA-NO (Figure 4C). Data demonstrate that decreased spare
298 respiratory capacity of *MtbΔsufR* increased its vulnerability towards
299 bioenergetic exhaustion under NO stress. However, unlike wt *Mtb*, *MtbΔsufR*
300 significantly increases basal ECAR and retains CCCP-induced ECAR in
301 response to 0.25 mM and 0.5 mM of DETA-NO (Figure 4D). This suggests an
302 increased reliance of *MtbΔsufR* on glycolysis to handle the bioenergetic
303 needs under NO stress. Lastly, using the Mrx1-roGFP2 biosensor, we
304 measured E_{MSH} of *MtbΔsufR* in response to NO. We observed that NO

305 induces a slightly higher oxidative shift in E_{MSH} of *MtbΔsufR* than wt *Mtb* in a
306 dose-dependent manner (Figure 4E). Consistent with this, staining with the
307 dye CellROX also indicated higher oxidative stress in NO-treated *MtbΔsufR*
308 as compared to wt *Mtb* (Figure 4F). Altogether, our data indicate that SufR is
309 required to regenerate Fe-S clusters, maintain respiratory reserves, and buffer
310 redox imbalance to counteract NO stress.

311

312 **SufR mediates adaptation to NO stress *in vivo***

313 Next, we investigated the biological consequence of compromised Fe-
314 S homeostasis and bioenergetics by assessing the phenotype of *MtbΔsufR*
315 under NO stress. A single dose of various concentrations of DETA-NO (0.5
316 mM, 1.25 mM, and 2.5 mM) did not influence the survival of *MtbΔsufR* (Figure
317 5A). Repeated exposure to low doses of NO is known to arrest the growth of
318 *Mtb* for an extended duration (44). Administration of 0.1 mM of DETA-NO
319 every 6 h for 36 h induces an extended period of growth arrest followed by
320 recovery of wt *Mtb* at day 7 post-treatment (Figure 5B). In contrast, *MtbΔsufR*
321 resumed growth only at day 16 post-treatment with NO (Figure 5C). The *sufR-*
322 *comp* strain showed a recovery defect similar to *MtbΔsufR*, indicating that the
323 NO-mediated induction of the entire *suf* operon rather than only *sufR* is
324 necessary for the timely resumption of growth. We confirmed this by depleting
325 an essential gene of *suf* operon (*Rv1466*; *sufT*) involved in Fe-S cluster
326 maturation (45) using CRISPR interference (CRISPRi-*sufT*). Reduced *sufT*
327 levels significantly delayed recovery of *Mtb* from NO-induced growth inhibition
328 (Figure 5C).

329

330 Immunologically activated macrophages are known to induce
331 nitrosative stress in *Mtb* (46). In line with this, *MtbΔsufR* showed 10- and 40-
332 fold reduced survival in immune-activated Raw264.7 macrophages as
333 compared to wt *Mtb* at day 2 and 4 post-infection, respectively (Figure 5D).
334 These observations prompted us to investigate the NO-dependent phenotype
335 of *MtbΔsufR in vivo*. WT *Mtb* and *MtbΔsufR* showed comparable growth in the
336 lungs of BALB/c mice during the acute phase of infection (0-2 weeks) (Figure
337 5E). However, *MtbΔsufR* was cleared progressively from the lungs, with a
338 more than 1.5-log decline in bacterial burden by 8 weeks (Figure 5E). The
339 persistence defect of *MtbΔsufR* was partially rescued in the case of animals
340 infected with *sufR-Comp* (Figure 5E). Since *sufR-Comp* did not restore the
341 induction of the *suf* operon, the partial complementation is likely due to
342 restored expression of other *sufR*-specific genes (*e.g.,* DosR regulon). The
343 histopathological changes observed in the lungs of animals at 8 weeks post-
344 infection were proportionate to the bacterial burden (Figure 5-figure
345 supplement 1A). The magnitude of pulmonary damage was highest in case of
346 wt *Mtb* (2.75±0.5), intermediate in *sufR*-Comp (2.0 ±0.0), and lowest in
347 *MtbΔsufR* (0.25±0.50) (Figure 5-figure supplement 1B). Lastly, to clarify the
348 role of NO in the persistence defect of *MtbΔsufR*, we infected a highly
349 susceptible mouse strain lacking inducible nitric oxide (iNOS$^{-/-}$) (5). We found
350 that the phenotypic defect of *MtbΔsufR* was abolished in iNOS$^{-/-}$ mouse,
351 indicating the requirement of SufR for the persistence of *Mtb* in response to
352 NO (Figure 5F-G).

353

354

355 **Mechanism of SufR mediated regulation of Fe-S biogenesis**

356 Having confirmed the role of SufR in regulating Fe-S homeostasis,
357 bioenergetics, and *in vivo* persistence, we next sought to understand the
358 underlying biochemical and molecular mechanisms. Biochemical
359 characterization of SufR revealed the presence of a 4Fe-4S cluster. We
360 present data to demonstrate how the 4Fe-4S cluster in SufR serves as a
361 sensor for NO and H_2O_2 to modulate DNA binding and transcriptional
362 activity. These studies, which also allowed us to identify the DNA sequence
363 motif required for SufR binding, provide a basis for a mechanistic model for
364 SufR. The data and analysis leading to this model are described below.

365

366 **SufR contains a 4Fe-4S cluster**

367 We anaerobically purified histidine-tagged SufR from *E.coli* cultured in
368 growth conditions optimized for the maximum incorporation of Fe-S clusters *in*
369 *vivo* (47). As isolated, native SufR displayed a characteristic straw brown
370 color, with an absorption maximum indicative of a 4Fe-4S cluster at 413 nm
371 (molar absorption coefficient [ε] at 413 =16200 M^{-1} cm^{-1}) (Figure 6A and
372 Figure 6-figure supplement 1) (18). Treatment of native SufR with a one-
373 electron donor, sodium dithionite (DTH), caused partial bleaching of brown
374 color and loss of absorbance at 413 nm, consistent with the presence of a
375 redox-responsive 4Fe-4S cluster (18) (Figure 6A). Gel-filtration performed
376 under anaerobic conditions suggested a molecular mass of ~ 54 kDa for
377 native SufR, which is consistent with a dimer. Clusterless SufR (apo-SufR)

378 also eluted as a dimer, indicating that the Fe-S cluster does not bridge SufR
379 monomers (Figure 6B). Moreover, the identity of cysteine residues that
380 coordinates the 4Fe-4S cluster were experimentally validated. The alanine
381 mutants of three putative cysteine ligands (C175A, C179A and C192A) were
382 seen to disrupt the 4Fe-4S cluster as evident from the loss of absorbance at
383 413 nm (Figure 6C).

384

385 A recent study, using aerobically purified SufR, has demonstrated that
386 SufR is a monomer and coordinates a 2Fe-2S cluster upon Fe-S cluster
387 reconstitution *in vitro* (39). Since Fe-S clusters are susceptible to O_2 (48), our
388 technique of assembling Fe-S cluster *in vivo* followed by anaerobic
389 purification is more likely to provide native configuration of SufR Fe-S cluster.
390 We clarified this by analyzing native SufR using circular dichroism (CD). The
391 far-UV CD spectrum shows two minima at 208 and 224 nm and indicates the
392 presence of 70% α-helical content in the secondary structure (Figure 6D). The
393 near-UV CD spectrum displayed two characteristic maxima at 330 and 420
394 nm and minima near 550 nm as described earlier for [4Fe-4S] cluster (Figure
395 6E) (49). As expected, the near-UV CD spectrum of apo-SufR did not show
396 the absorption characteristics of a [4Fe-4S] cluster (Figure 6E). Lastly, the
397 estimation of iron and sulfide ions in the native SufR revealed the association
398 of 3.23-3.75-iron atoms/SufR monomer and similar amounts of sulfide
399 ion/SufR monomer (Figure 6F). In sum, we demonstrate that *Mtb* SufR
400 contains a 4Fe-4S cluster.

401

402 **SufR responds to NO through its 4Fe-4S cluster**

403 We exposed native SufR to the fast releasing NO donor; proline
404 NONOate ($T_{1/2}$ ~ 1.8 s, pH 7.4) and subjected it to UV-visible spectroscopy.
405 Treatment with proline NONOate gradually reduced absorbance at 413 nm
406 and formed a new chromophoric feature at ~ 350 nm over time with a clear
407 isosbestic point (Figure 7A). These spectral features are consistent with a
408 dinitrosyl-iron dithiol complex (DNIC), wherein the sulfide ligands of the 4Fe-
409 4S clusters are displaced by NO to form [Fe-$(NO)_2$] (50). The DNIC formation
410 was confirmed by subjecting NO-treated SufR to continuous wave Electron
411 Paramagnetic Resonance (cw-EPR). A strong EPR signal centered at *g*=2.03
412 was observed in a dose-dependent manner, consistent with the formation of
413 the monomeric DNIC complex on SufR (Figure 7B) (18).

414

415 The *suf* operon showed induction under oxidizing stress (*e.g,* H_2O_2) (51).
416 Therefore, we determined whether the Fe-S cluster of SufR is responsive to
417 O_2 and H_2O_2. Exposure to atmospheric O_2 resulted in a slow decline in
418 absorbance at 413 nm (Figure 7C). A plot of ΔA_{413nm} against time revealed
419 the loss of ~75% of the 4Fe-4S cluster only at 20 hr post-O_2 exposure.
420 However, exposure of native SufR to 1 mM H_2O_2 resulted in the rapid loss of
421 absorption at 413 nm (Figure 7D). A plot of ΔA_{413nm} against time revealed
422 the loss of ~75% of the 4Fe-4S cluster in 20 min. Higher concentrations of
423 H_2O_2 (10 mM and 100 mM) resulted in the loss of the cluster within 1-2 min
424 (Figure 7-figure supplement 1A-C). Taken together, these data demonstrate
425 that the 4Fe-4S cluster of SufR is sensitive to NO and H_2O_2.

426

427 **SufR binds upstream of the *suf* operon promoter and represses**
428 **expression**

429 To investigate the DNA binding properties of SufR, we carried out
430 electrophoretic mobility shift assays (EMSA) using a radioactively (^{32}P)
431 labeled 170 bp DNA fragment encompassing the promoter region of *suf*
432 operon (39). We used four different forms of SufR; native/holo-SufR, apo-
433 SufR, NO-treated SufR, and H_2O_2-treated SufR. As shown in figure 8a, holo-
434 SufR binds to the *suf* promoter region in a concentration-dependent manner,
435 whereas apo-SufR, NO-treated SufR, and H_2O_2-treated SufR show no DNA
436 binding (Figure 8A-C). Moreover, DNA binding was outcompeted by 50-100-
437 fold excess of unlabeled *suf* promoter DNA, but not by an unrelated promoter
438 fragment (*blaC*) (Figure 8D). These findings suggest that *Mtb* SufR is an NO-
439 and H_2O_2-responsive, sequence-specific DNA binding protein.

440

441 We next performed *in vitro* transcription using *Mtb* RNA polymerase as
442 described (52). Single round of transcription of the *suf* promoter fragment (180
443 bp [-73 to + 107 bp]) produced a single transcript of 107 nucleotides,
444 consistent with the leaderless transcription of the *suf* operon (53). Addition of
445 holo-SufR represses transcription from the *suf* promoter in a dose-dependent
446 manner, whereas apo SufR does not (Figure 8E-F). Importantly, the treatment
447 of holo-SufR with proline NONOate (NO) reversed the repression of *suf*
448 promoter (Figure 8G). These results indicate that holo-SufR binds to the *suf*
449 promoter and represses expression, whereas NO-damaged or clusterless

450 apo-SufR lacks DNA binding and transcription repression. The data suggest
451 that occupancy of Fe-S cluster on SufR serves as an indicator of Fe-S cluster
452 sufficient or deficient conditions. During low Fe-S cluster demand, holo-SufR
453 represses the Suf system to reduce Fe-S cluster assembly, whereas loss or
454 damage of the Fe-S cluster in SufR signals heightened demand for Fe-S
455 clusters that results in the de-repression of the *suf* operon and mobilization of
456 Fe-S cluster assembly. In support of this, limiting Fe-S cluster biogenesis by
457 depleting SufT (CRIPSRi-*sufT*) alleviates the SufR-dependent repression of
458 the *suf* operon in *Mtb*, suggesting that *suf* machinery assembles the Fe-S
459 cluster on SufR to regulate Fe-S homeostasis (Figure 8-figure supplement 1).

460

461 Lastly, we performed DNase I footprinting to identify the binding site of
462 native SufR on the promoter region of the *suf* operon (Figure 9). A clear
463 region of protection from DNase I digestion was evident with increasing molar
464 ratios of SufR:DNA (Figure 9A-B). The protected region contains a perfect
465 inverted repeat (**ACACT**-N_5-**TGTGA)** that is separated by 5 bp (Figure 9).
466 This inverted repeat forms a part of a larger inverted repeat
467 (**ATTTT**GTCACACT-N_5-TGTG**AAAAT**). Consistent with the footprinting data,
468 mutations in the inverted repeat completely abolished binding, thus confirming
469 that the SufR binds the palindrome **ACACT**-N_5-**TGTGA** (Figure 9C-E). This
470 palindromic sequence was found to be present upstream of ~ 10 genes
471 deregulated in *MtbΔsufR* under NO stress (Supplementary file 2). Altogether,
472 using multiple techniques we confirmed that SufR functions as a NO- and
473 H_2O_2-sensitive DNA-binding transcription factor in *Mtb*.

474

475 **Discussion**

476 Fe-S cluster production is tightly regulated to promote Fe-S
477 formation when the necessity for the clusters is heightened (*e.g.,* ROI/RNI/iron
478 limitation) and to limit unnecessary production when the demand is low (*e.g.,*
479 hypoxia) (54). Deregulation of Fe-S cluster biogenesis can lead to toxic
480 accumulation of iron and polysulfides inside cells (54). Therefore, calibrated
481 expression of Fe-S cluster biogenesis is important. Here we show that *Mtb*
482 SufR a major regulator of Fe-S cluster biogenesis in *Mtb* under NO stress. We
483 provided biochemical evidence that *Mtb* SufR contains a redox-responsive
484 4Fe-4S cluster that reacts with NO to form a DNIC complex. We also
485 establish a link between NO, Fe-S biogenesis, respiration, and SufR. Our
486 findings provide a new mechanistic insight into how *Mtb* exploits Fe-S cluster
487 regulation and biogenesis processes under NO stress to favor the pathogen's
488 persistence.

489

490 Our RNA-seq data revealed a major realignment of expression of
491 genes encoding Fe-S cluster proteins and Fe-S cluster biogenesis (*suf*
492 operon) in NO-treated *Mtb*. Reduced expression of Fe-S cluster factors
493 associated with energy generation (*e.g.,* TCA cycle and primary respiration)
494 indicates that metabolic constraints imposed by NO represent the proximal
495 cause of growth arrest in *Mtb*. Moreover, while the majority Fe-S cluster
496 proteins are degraded in NO-stressed *Mtb* (13), Suf proteins remained
497 induced, suggesting that the *suf* operon is likely to facilitate regeneration of
498 Fe-S clusters during recovery from NO stress. This is reinforced by our data
499 showing an excellent recovery of Acn activity upon removal of NO stress in

500 case of wt *Mtb* but not in *MtbΔsufR* cells. Likewise, recovery from NO-
501 mediated growth arrest was significantly delayed in *MtbΔsufR*. Given the
502 strong reactivity of NO to metabolic and respiratory enzymes coordinating Fe-
503 S clusters and heme-Fe (55), we observed major changes in bacterial
504 OXPHOS, ECAR, and E_{MSH}, suggesting that NO-mediated cytostasis is
505 coupled to changes in redox balance and bioenergetics in *Mtb*. Our seahorse
506 XF flux data provide new insights into the mechanisms of NO-mediated
507 respiratory arrest in *Mtb*.

508

509 We discovered that under low electron (e^-) flux and high O_2
510 conditions (basal respiration), NO stimulated OCR possibly by collapsing
511 proton motive force (PMF). This is in agreement with the role of NO in
512 depolarizing the cytoplasmic membrane to arrest respiration and growth
513 (56,57). Upon artificially increasing the e^- flux through the respiratory chain
514 (CCCP treatment), which also depletes O_2 (58), NO efficiently inhibited O_2
515 consumption and depleted spare respiratory capacity of *Mtb*. In line with this,
516 the transcriptome of *Mtb* is remarkably responsive to NO under O_2 limitation
517 (2). We also found that spare respiratory capacity of *MtbΔsufR* is more
518 severely inhibited by NO as compared to wt *Mtb*. Since spare respiratory
519 capacity depends mainly on the recruitment of previously inactive respiratory
520 complexes (59), the sustained activation of the SUF system can provide a
521 reserve of Fe-S cluster-containing respiratory complexes to maintain electron
522 transfer in response to NO. Induction of the *suf* operon in response to
523 conditions that damage Fe-S clusters (*e.g.,* H_2O_2, NO, iron-starvation,

524 antibiotics, phagosomal pH, and sputum) (40,51,52,60-64) indicates that *Mtb*
525 relies on Suf-dependent Fe-S cluster coordination to maintain persistence.

526

527 Our biochemical data support the role of SufR in sensing and
528 activating Fe-S cluster biogenesis under unfavorable conditions. For example,
529 H_2O_2 and NO rapidly targeted the 4Fe-4S cluster of SufR, whereas O_2 was
530 extremely sluggish. In agreement with this, Acn activity was largely unaffected
531 in *MtbΔsufR* under aerobic conditions but was significantly perturbed following
532 exposure to NO. Interestingly, a stand-alone *Mtb* cysteine desulfurase (IscS)
533 likely coordinates Fe-S clusters of Acn and succinate dehydrogenase under
534 aerobic conditions (65). Data suggest that *Mtb* prefers IscS for housekeeping
535 functions but the Suf system for managing stress. Similar roles were assigned
536 for IscS and Suf systems in *E. coli* (54). From the regulation perspective, SufR
537 appears to coordinate the expression of the *suf* operon in a negative feedback
538 loop. Holo-SufR serves as an indicator of Fe-S cluster sufficiency and
539 represses the *suf* operon, whereas apo- or DNIC forms of SufR indicate Fe-S
540 deficiency, resulting in derepression of the *suf* operon. Once the Fe-S cluster
541 demands are satisfied, the *suf* system reconstitutes the Fe-S cluster of SufR
542 to maintain homeostasis. We propose that this carefully choreographed
543 mechanism allows *Mtb* to calibrate Fe-S cluster supply with demand in
544 response to environmental signals encountered during infection, as shown
545 schematically in figure 10.

546

547 The marginal survival defect of *MtbΔsufR* inside resting
548 macrophages and during early stages of infection *in vivo* indicates a lower
549 requirement of *suf*-dependent Fe-S biogenesis or possible compensation by
550 IscS. Consistent with this, *MtbΔsufR* showed attenuated phenotype inside the
551 nitrosatively hostile environment of activated macrophages and chronically
552 infected lung tissues. Both of these microenvironments are likely to increase
553 the demand for Fe-S cluster biogenesis. The capacity of SufR to sense and
554 respond to a range of cues, such as NO, H_2O_2, and iron limitation, possibly
555 empowers *Mtb* to transduce different redox signals into transcriptional
556 responses crucial for persistence *in vivo*. The overexpression of the DosR
557 regulon in *MtbΔsufR* relative to wt *Mtb* specifically under NO stress indicates
558 that SufR-mediated gene regulation extends beyond derepression of the *suf*
559 operon. Interestingly, the *suf* operon was overexpressed in *MtbΔdosR* under
560 hypoxia (15), signifying a regulatory loop between SufR and DosR in *Mtb*.
561 This is supported by our *in vivo* data wherein the persistence defect displayed
562 by *MtbΔsufR* was partially restored in *sufR*-Comp even though the expression
563 of the *suf* operon was not reinstated. Interestingly, the expression of the DosR
564 regulon recovered to wt levels in *sufR*-Comp, suggesting that further work is
565 required to explore the breadth of SufR-mediated gene regulation. Based on
566 this cumulative evidence, we propose that *Mtb* SufR senses NO through its Fe-S cluster
567 to coordinate Fe-S cluster biogenesis and regulate metabolism, respiration, and redox
568 balance for long-term persistence.

569

570

571

572 **Materials and Methods:**

573 **Culture Conditions**. The *Mtb* H37Rv, *MtbΔsufR,* and *sufR*-comp
574 were grown in Middlebrook 7H9 broth (Becton, Dickinson and Company (BD),
575 USA) medium supplemented with 0.2% glycerol, 0.5% BSA, 0.2% dextrose,
576 and 0.085% NaCl (ADS) with 0.05% Tween 80 as described previously (40).
577 For culturing on solid medium, *Mtb* strains were cultured on 7H10/7H11 agar
578 medium (Becton, Dickinson and Company (BD), USA) supplemented with 1x
579 OADC (Becton, Dickinson and Company (BD), USA) and 0.2% glycerol. *E.*
580 *coli* cultures were grown in LB medium (HIMEDIA, India). Whenever required,
581 antibiotics were added to the culture medium (for *E. coli*, 100 µg/ml
582 kanamycin (Amresco, USA) and 150 µg/ml hygromycin (Sigma-Aldrich, India);
583 for *Mtb* strains, 50 µg/ml hygromycin).

584

585 **RNA Sequencing experiments**:

586 The *Mtb* strains were grown to an $O.D._{600}$ of 0.4 and exposed to 0.5
587 mM diethylenetriamine-nitric oxide (DETA/NO [Sigma-Aldrich, India]) for 4 h at
588 37°C. The experiment was carried out with three independent biological
589 replicates. Total RNA extraction was conducted using the FastRNA® Pro Blue
590 Kit (MP Biomedicals, USA) in accordance with the manufacturer's instruction
591 and further purified using RNeasy spin columns (Qiagen, USA) as described
592 (40). Following purification, the RNA was quantified and assessed for purity
593 by a 2100 Bioanalyzer (Agilent Technologies, Waldbronn, Germany). RNA
594 samples with an RIN (RNA Integrity Number) value >8 were processed further
595 for sequencing. Ribosomal RNA (16s and 23s rRNA) was removed by

596 hybridization with magnetic beads-coupled oligonucleotide (MicrobExpress
597 Kit, Life Technologies, USA) and concentration of enriched mRNA was
598 quantified by QuBit RNA HS Assay Kit (Life Technologies, USA). RNA-seq
599 was performed as described (17). In brief, libraries were prepared using
600 NEBNextUltra Directional RNA Library Prep Kit for Illumina' (New England
601 Biolabs, USA), according to manufacturer's instructions. The library size
602 distribution and quality were assessed using a high sensitivity DNA Chip
603 (Agilent Technologies, USA) and sequenced in HiSeq 2500 platform (Illumina,
604 USA) sequencer using 1X50 bp single-end reads with 1% PhiX spike-in
605 control.

606

607 **Differential gene expression and statistical analysis for RNA-Seq:**

608 Raw reads were obtained for *Mtb* H37Rv strain as fastq files. The
609 reference genome sequence (.fna) and annotation (.gff) files for the same
610 strain (accession number: NC_000962.3) were downloaded from the ncbi ftp
611 website ("ftp.ncbi.nlm.nih.gov"). The annotation file was customized with the
612 addition of annotations for non-coding RNAs (66). The format of the
613 annotation file (.gff) was changed to .bed using an in-house python script. The
614 raw read quality was checked using the FastQC software (version v0.11.5;
615 http://www.bioinformatics.babraham.ac.uk/projects/fastqc). BWA (version
616 0.7.12-r1039)(67) was used to index the reference genome. Reads with raw
617 read quality >= 20 were aligned using BWA aln -q option. SAMTOOLS
618 (version 0.1.19-96b5f2294a) (68) was used to filter out the multiply mapped
619 reads. BEDTOOLS (version 2.25.0)(69) was used to calculate the reads count
620 per gene using the annotation file (.bed). The normalization and differential

621 gene expression analysis for the conditions were carried out using edgeR as
622 mentioned previously (70). Genes with at least 10 reads were selected for
623 each comparative analysis. DGE analysis was done in RStudio (1.1.447) with
624 R version 3.4.4. (http://www.rstudio.com/)
625

626 **Aconitase assay:**

627 The activity of aconitase (Acn) was measured by monitoring the
628 disappearance of cis-aconitate at 240nm in a UV spectrophotometer (Thermo
629 Scientific Biomat 3S, USA) as described (71). One unit (U) of aconitase
630 activity is defined as 1μmol cis-aconitate formed or converted per minute.
631 Reaction mixtures (1ml) for Acn contained 25mM Tris-HCl (pH 8.0), 100 mM
632 NaCl, and 50 μg *Mtb* cell lysates. Reactions were initiated by adding 0.15 mM
633 cis-aconitate and monitored by following the disappearance of cis-aconitate at
634 240 nm after every 15 sec for total 30 min. Absorbance at 240 was plotted
635 against time. Acn activity was calculated from linear portion of the curve in
636 initial 5 min when reaction follows 0th order of reaction. An extinction
637 coefficient of 3,500 $M^{-1}cm^{-1}$ was used to calculate the rates.

638

639 **Western blot:**

640 Whole cells lysate (50 μg) was separated on 12% SDS-PAGE
641 and then transferred onto a PVDF membrane (GE Healthcare, Piscataway,
642 NJ, USA). Membrane were blocked in 5% (w/v) nonfat dry milk and incubated
643 for 3 h at room temperature with primary antibody (Acn and Cbs 1:10000
644 dilution). After washing with 1XTBST, membranes were incubated in goat

645 anti-rabbit IgG HRP-conjugated secondary antibody (1:10000 dilution) for 1 h.
646 The autoradiography signals were visualized using ECL advance Western
647 blotting detection kit (BioRad, USA).

648

649 **OCR and ECAR measurements:**

650 The *Mtb* strains adhered to the bottom of a XF cell culture
651 microplate (Agilent technologies, USA), at $2X10^6$ bacilli per well by using Cell-
652 Tak (a cell adhesive). OCR and ECAR were measured using Agilent XF
653 Extracellular Flux Analyser. Assays were carried out in unbuffered 7H9 media
654 (pH 7.35) with glucose 2mg/ml as carbon source. Basal OCR and ECAR were
655 measured for initial 21 min before the automatic addition of freshly prepared
656 DETA-NO (0 mM, 0.25 mM, 0.5 mM and 1 mM) in 7H9 unbuffered media,
657 through port A of cartridge plate. Three measurements were taken after 1 h of
658 incubation. CCCP (Sigma-Aldrich, India) was added at 10 μM concentration to
659 achieve maximum rate of respiration. Raw data of OCR and ECAR was CFU
660 normalised for $2X10^6$ CFU/ well. Spare respiratory capacity, was calculated
661 from % OCR value, by subtracting third basal reading (normalized as 100%)
662 from first point after CCCP addition.

663

664 **CellRox Deep Staining and Flow Cytometry:**

665 Logarithmically grown *Mtb* strains were treated with DETA-NO (0
666 mM, 0.25 mM, 0.5 mM and 1 mM) and then incubated at 37 °C with shaking
667 for 2 h. 200 μl cells were treated with CellROX® reagent (Thermo Fisher,
668 USA) at a final concentration of 5 μM for 30 minutes at 37°C and analysed on

669 BD FACSVerse flow cytometer with 640/665 nm excitation and emission
670 respectively. We collected 5000-10,000 events for each sample wherever
671 possible.

672

673 **Animal experiments:**

674 For the chronic model of infection, 5- to 6-week-old female
675 BALB/c, C57BL/6 and iNOS$^{-/-}$ mice (n = 6 per group) were infected by aerosol
676 with approximately 100 bacilli per mouse with the *Mtb* strains using a Madison
677 chamber aerosol generation. At indicated times post infection, mice were
678 euthanized, and the lungs were harvested for bacillary load, tissue
679 histopathology analysis, and pathological scoring as described (40). The
680 remaining tissue samples from each mouse were homogenized and bacillary
681 load was quantified by plating serial dilutions of tissue homogenates onto
682 Middlebrook 7H11-OADC agar plates supplemented with lyophilized BBL
683 MGIT PANTA antibiotic mixture ((polymyxin B, amphotericin B, nalidixic acid,
684 trimethoprim, and azlocillin, as supplied by BD;USA). Colonies were observed
685 and counted after 4 weeks of incubation at 37°C.

686

687 **Construction of *Mtb* SufT Knock Down strain:**

688 For construction of *Mtb* SufT Knock Down strain **(**SufT KD), we
689 have followed CRISPR interference (CRISPRi) technology was utilized as
690 described (72). Anhydrotetracycline (ATC, Cayman, USA) 200 ng/ml was
691 added for the induction of *sufT* specific–guide RNA (sgRNA) and dCas9 every
692 48 h. SufT KD culture was divided equally when A_{600} reached 0.1–0.2 and

693 cultured in the presence or absence of ATC. The dCas9 was expressed by
694 pRH2502 from a TetR-regulated *uvtetO* promoter and sgRNA in pRH2521
695 under the control of a TetR-regulated *smyc* promoter (Pmyc1tetO). To deplete
696 *sufT,* gene specific sgRNAs were designed for two regions between 98-127
697 bp and 171-191 bp of *sufT* and cloned in pRH2521. Depletion of *sufT* was
698 verified by qRT-PCR and based on the significant repression of *sufT,* we
699 chose sgRNA targeting *sufT* region between 98-127 bp for further study. For
700 qRT-PCR analysis, total RNA was extracted from SufT KD and control strains
701 after 24 h of ATC treatment. After DNase treatment, total 600 ng of RNA was
702 used for cDNA synthesis by using Random hexamer oligonucleotide primer
703 (iScript Select cDNA Synthesis Kit, BioRad, USA). Gene specific primers
704 (Supplementary file 3) and iQ SYBER Green Supermix (BioRad, USA) were
705 used for RT-PCR (StepOne Plus, Thermo, USA). Gene expression was
706 normalized to *Mtb* 16S rRNA expression level.

707

708 **NO exposure and recovery:**

709 Logarithmically grown *Mtb* strains (OD_{600} of 0.8) were diluted to an
710 OD_{600} of 0.1 and exposed to six doses of 100 μM DETA-NO, once every 6 h.
711 Recovery from exposure to DETA-NO was monitored by recording the
712 OD_{600} after each addition of DETA-NO, as well as every 24 h after addition.
713 Two biological replicates were used for each strain. For single dose
714 experiments, different doses of DETA-NO (0.5 mM, 1.25 mM, 2.5 mM and
715 1mM) were added. After 4 and 24 h cells were harvested, washed with 1X
716 PBS and plated on ADS-7H11 plates. Colonies were counted after 3–4 weeks
717 of incubation at 37°C.

718

719 **Cell line experiments:**

720 RAW 264.7 murine macrophage cell line was activated by
721 treatment with IFN-Y (100U/mL, Invitrogen, USA) for 12 h before infection and
722 LPS (100 ng/mL, Sigma-Aldrich, India) for 2 h before infection. Activated RAW
723 264.7 macrophages were infected with wt *Mtb*, *MtbΔsufR*, and *sufR-Comp*
724 strains at multiplicity of infection (MOI) 2 for 4 h, followed by washing
725 thoroughly to remove extracellular bacteria with warm DMEM medium and
726 suspended in the same containing 10 % FBS. For CFU determination
727 macrophages were lysed using 0.06 % SDS-7H9 medium diluted in
728 PBS/Tween and plated on OADC-7H11 at indicated time points. Colonies
729 were counted after 3–4 weeks of incubation at 37°C.

730

731 **Purification of SufR under anaerobic conditions:**

732 The entire ORF of *Mtb sufR* (Rv1460) was PCR-amplified using gene-
733 specific oligonucleotides (pET28a*sufR*F and pET28a*sufR*R; Supplementary
734 file 3), digested with *Nde*I-*Hind*III, and ligated into similarly digested His-tag-
735 based expression vector, pET28a (TAKARA BIO, Clontech Laboratories, CA,
736 USA) to generate pET28a:SufR. A N-terminal histidine-tagged SufR was
737 overexpressed in *E. coli* BL21 λDE3 by 0.6 mM IPTG [Isopropyl β- d-1-
738 thiogalactopyranoside; MP Biomedicals, USA (60 min, 30 °C)]. To facilitate
739 Fe-S cluster formation, cultures were incubated on ice for 18 min prior to
740 induction and were supplemented with 300 μM Ferric ammonium citrate and
741 75 μM L- Methionine (Amresco, USA) and purified as described (47).

742 Purification was performed under strict anaerobic conditions inside an
743 anaerobic glove box (PLas-Labs, Lansing, MI, USA) maintaining ≈2.0 ppm O_2
744 by volume, and buffers and solutions were appropriately deoxygenated. The
745 *sufR* gene on pET28a-SufR was mutated using oligonucleotide-based site-
746 directed mutagenesis approach to create individual cysteine to alanine
747 substitutions. After the PCR, *Dpn*I was added into the reaction mixture to
748 digest the wild- type plasmid that was used as the template. The reaction
749 mixture containing the mutated *sufR* gene was used to transform *E. coli* BL21
750 λDE3. Sequences of primers used to create mutations are shown in (Data set
751 1F). Resulting clones were verified by sequencing, and the mutant Cys
752 variants of the wt SufR were purified as described earlier. In order to generate
753 apo-SufR, the holo-SufR was incubated with EDTA
754 (Ethylenediaminetetraacetic acid, Sigma-Aldrich, India) and potassium
755 ferricyanide in a molar ratio of protein: EDTA: ferricyanide in 1:50:20 at 25°C
756 and incubated for 20-30 min till the extensive loss of color. The solution was
757 passed through PD10 desalting column and stored at -80 °C.

758

759 **UV-Vis, CD analysis, and gel filtration of SufR:**

760 The UV-visible absorption spectroscopy was carried out in a
761 Thermo scientific spectrophotometer (Thermo scientific, USA) at 25°C.
762 Absorption spectra of SufR WT (native/holo) and mutants were recorded
763 immediately as the elution fractions were collected during the purification. In
764 order to study the effect of air oxidation, on Fe-S cluster stability, freshly
765 purified holo-SufR was transferred to an anaerobic quartz cuvette, exposed to
766 air by opening the cap and mixing by pipetting for 2 min. The cuvette was then

767 sealed and monitored by UV-visible spectroscopy over time (Thermo
768 scientific, USA). To study the effect of NO, DTH and H_2O_2 on [4Fe-4S] cluster
769 of SufR, the absorption spectra of freshly purified protein were recorded at
770 indicated concentration and different time intervals in anaerobic quartz
771 cuvette.

772

773 CD measurements were conducted in a Jasco J-715
774 spectropolarimeter (Jasco, USA). Far-UV spectra were measured from 190 to
775 250 nm range and near-UV spectra from 300 nm to 650 nm range. Protein
776 concentration used for the far-UV CD measurements was 10-20 μM and for
777 the near-UV measurements 140-150 μM. Cells of 1.0 cm path length were
778 used for the measurements of the far- and near-UV spectra, respectively.
779 Three repeat scans were obtained for each sample. The averaged baseline
780 spectrum was subtracted from the averaged sample spectrum. The protein
781 was dissolved in 5 mM phosphate buffer pH 7.4and 150 mM NaCl. Results
782 are expressed as molar ellipticity [θ] (deg cm2 dmol-1), calculated from the
783 following formula $[\theta]\lambda=\theta/[c]*l*10*n$, where, θ is the measured ellipticity in
784 degrees at wavelength λ, c is the protein concentration in mgml-1, l is the light
785 path length in centimeters and n is the number of amino acids. CD Pro
786 software was used to analyze the data.

787

788 To determine the molecular mass of apo- and holo-SufR protein,
789 analytical size-exclusion chromatography experiments were performed with
790 Superdex 200 increase, 10/300 GL analytical column (GE Healthcare Life

791 Sciences, USA). The column was pre-equilibrated and eluted with the running
792 buffer (10 mM phosphate buffer, 10% glycerol and 100 mM NaCl at pH 7.4) at
793 a constant flow rate of 0.5 ml/min. Molecular mass of the proteins was
794 determined by using gel filtration molecular mass standard (Carbonic
795 Anhydrase, Albumin, Alcohol Dehydrogenase, β-Amylase, Apoferritin and
796 Thyroglobulin). Ve/Vo was plotted as a function of log10 Mr of the standard
797 protein where Ve is the elution volume of the protein, V0 is the void volume of
798 the column and Mr molecular weight of the particular protein. Blue dextran
799 was used to determine the void volume (Vo). Running buffers were purged
800 with nitrogen gas and were degassed thoroughly to remove any dissolved
801 atmospheric oxygen. The experiments were conducted under anaerobic
802 conditions.

803

804 **EPR spectroscopy of SufR:**

805 For EPR spectroscopy, Holo SufR was treated inside the
806 anaerobic glove box with aliquots of freshly prepared proline NONOate
807 (Cayman Chemicals, Ann Arbor, MI, USA). Aliquots of SufR were placed in an
808 anaerobic cuvette and titrated by injection with aliquots of a 2.5 mM stock
809 solution of proline NONOate (Cayman chemicals, USA). Samples were then
810 transferred to EPR tubes and immediately frozen in liquid nitrogen. EPR
811 characteristics of NO-treated SufR were analyzed by subjecting the samples
812 to continuous-wave spectrometers at liquid nitrogen temperature as described
813 previously (18). NO-treated SufR was analyzed by continuous-wave EPR on a
814 perpendicular mode X-band EPR spectrometer operating at 100-kHz
815 modulation frequency and equipped with liquid nitrogen cryostat and a dual

816 mode X-band cavity (JES200 ESR spectrometer, JEOL, USA). Field
817 calibration was done by using a standard NMR G meter. The background
818 signal from the buffer was subtracted from the spectra.

819

820 **Chemical analysis of Iron and Sulfide:**

821 The total iron content and acid-labile sulfide content of holo-SufR, was
822 measured using a previously described procedure (73). For iron estimation,
823 freshly purified holo-SufR (0.1 mL) was heated at 95°C degree for 30 min
824 after treatment with 22% HNO_3 (0.1 mL). Samples were cool to ambient
825 temperature followed by addition of 0.6 mL ammonium acetate (7.5 % w/v),
826 0.1 mL freshly prepared ascorbic acid (12.5% w/v) and 0.1mL ferene (10
827 mM). The concentration of iron present in the protein was determined by
828 measuring the absorbance of the product, iron- ferrene complex at 593 nm,
829 which was compared with a standard curve prepared from dilutions of freshly
830 prepared Fe (III) solution in the range of 0-200 μM. To measure acid-labile
831 sulphide content, freshly prepared $Na_2S.9H_2O$ solution was used to prepared
832 standard solution in the range of 52-260 μM of S^{2-}. Protein sample / standard
833 (200 μL) was mixed with 0.6 mL of zinc acetate (1% w/v) followed by addition
834 of 50 μL of NaOH (12 %w/v). After incubation of 15 min, 0.15 mL of N, N-
835 dimethyl-p-phenylenediamine dihydrochloride (0.1 % w/v dissolved in 5 M
836 HCl) and 0.15 mL of freshly prepared 10 mM $FeCl_3$ (dissolved in 1M HCl) was
837 added. The reaction mixture was further incubated for 30 min at room
838 temperature and the absorbance of the product methylene blue was
839 measured at 670 nm. For iron and sulfide estimation three independent

840 preparation of holo-SufR were analyzed to ensure the reproducibility and
841 three dilution of each sample were considered.

842

843 **Electrophoretic mobility shift assays (EMSA):**

844 For EMSA promoter fragment of *sufR* (170 bp upstream of ATG)
845 and *blaC* (200 bp upstream of ATG) were PCR amplified from the *Mtb*
846 genome. The 5' end was labeled by [Y-32_P]-ATP using T4 polynucleotide
847 kinase (MBI Fermentas, USA) as per the manufacturer's instructions. The
848 labeled oligonucleotides were passed through a 1 mL Tris-EDTA, pH 7.5
849 equilibrated Sephadex G-50 column and elute was vacuum dried. Blunt ended
850 duplex DNA was prepared by annealing radiolabelled and complementary
851 cold oligonucleotides in a 1: 2 molar ratio in 50 µL reaction system containing
852 TE and 1X saline-sodium citrate buffer (3 M sodium chloride and 0.3 M
853 sodium citrate). The reaction mixture was heated to 95 °C for 5 min and then
854 cooled in a thermal cycler. Annealed mixtures were resolved by 10% native
855 PAGE in 1x Tris-borate EDTA (TBE). Assembled DNA substrates were
856 visualized on an X-ray film and substrates were subsequently purified by
857 excising the respective desired bands. DNA substrates were eluted by
858 incubating corresponding gel pieces in TE at 4°C for 6 h. Binding reactions
859 were performed in Binding buffer (25mM Tris-HCl, 1mM DTT, 0.1 mg/ml BSA,
860 5 mM $MgCl_2$; pH 7.4) for 30 min at 4°C and 6% polyacrylamide gel was used
861 to resolve protein-DNA complexes in an anaerobic chamber by
862 electrophoresis at constant voltage (50 V). 0.5 nM ^{32}P-labeled DNA substrates
863 were incubated with indicated concentrations of various forms of SufR (apo-,
864 holo-, H_2O_2-treated, and NO-treated). For competition with unlabeled DNA,

865 fragments of *sufR* and *blaC* (~200–250 bp upstream of translational start
866 codon) were PCR amplified from the *Mtb* genome and used in various
867 amounts to outcompete binding of holo-SufR to ^{32}P-labelled DNA fragments.
868 Gels were exposed to auto radiographic film and visualized by a phosphor
869 imager (Typhoon FLA-9000, GE Healthcare Life Sciences, USA). All the
870 above reaction and separation were performed under anaerobic condition
871 inside glove box (Plas-Labs, Lansing, MI, USA).

872

873 ***In vitro* transcription assays:**

874 The DNA templates (180 bp) including the *sufR* promoter regions
875 were PCR amplified using primers P*sufR* F1/P*sufR* R1 (Supplementary file 3).
876 The amplicons (50 nM) were pre-incubated with different concentration of
877 holo- and apo-SufR in the transcription buffer (50 mM Tris HCl, (pH 8.0), 10
878 mM magnesium acetate, 100 mM EDTA, 100 mM DTT, 50 mM KCl, 50 mg/ml
879 BSA, and 5% glycerol) for 30 min at room temperature. Single-round
880 transcription reactions were initiated with the addition of 100 nM *Mtb* RNAP-
881 σA holo enzyme, 100 μM NTPs, 1 μCi [α-32P]-UTP, 50 μg ml−1 heparin and
882 incubated at 37°C for 20 min. The reactions were terminated by addition of 2X
883 formamide dye (95% formamide, 0.025% (w/v) bromophenol blue, 0.025%
884 (w/v) xylene cyanol, 5 mM EDTA and 0.025% SDS and 8 M urea) and heated
885 at 95℃ for 5 min followed by snap chilling in ice for 2 min. The transcripts
886 were resolved on an 8% TBE-urea-PAGE gel. To study the effect of NO,
887 transcription assays were performed as mention above after treating the holo-
888 SufR with proline NONOate for 5 min followed by purification. All the

889 treatments and the reaction were performed inside anaerobic glove box under
890 anoxic condition.

891

892 **DNase I Footprinting:**

893 Five nanomolar of ^{32}P-labeled DNA substrate was incubated with
894 increasing concentration of purified holo-SufR in binding buffer (25 mM Tris-
895 HCl (pH 7.5), 1 mM DTT, 100 µg/ml BSA, 5 mM MgCl2, 5 mM CaCl2), and
896 samples were incubated for 30 min at 4 °C inside glove box under anaerobic
897 condition. Reactions were initiated by the addition of DNase I to a final
898 concentration of 0.05 units and incubated for 2 min at room temperature. The
899 reactions were terminated by the addition of 150 µL of TE (pH 7.5) followed by
900 incubation at 75°C for 15 mins to deactivate DNase I enzyme. The sample
901 was further subjected to vacuum evaporation and the pellet thus obtained was
902 re-suspended in loading dye (80% (v/v) formamide, 0.1% (v/v) BPB, and 0.1%
903 (v/v) xylene cyanol) and analyzed on a denaturing 15% polyacrylamide gel
904 containing 7M urea. The gel was dried, and the bands were visualized with a
905 Typhoon FLA-9000 phosphor imager (GE Healthcare Life Sciences, USA).
906 Maxam and Gilbert A + G ladder was prepared as described previously (74).

907 A custom python script was developed to search for the SufR binding site and
908 find its relative positions with respect to genes across the genome. A
909 sequence of 15 nt length was searched in the region 500 bp upstream of the
910 start codon and considered as a potential SufR binding site if it shares 80%
911 identity with 'ACACT' or 'TGTGA' at the ends.

912

913 **Ethics:**

914 Animal experimentation: This study was carried out in strict accordance
915 with the guidelines provided by the Committee for the Purpose of Control and
916 Supervision on Experiments on Animals (CPCSEA), Government of India.
917 The protocol of animal experiment was approved by animal ethical Committee
918 on the Ethics of Animal Experiments, Indian Institute of science (IISc),
919 Bangalore, India (Approval number: CAF/Ethics/544/2017). All efforts were
920 made to minimize the suffering.

921

922 **Statistical Analysis:**

923 All data were graphed and analyzed with Prism v8.0 (GraphPad)
924 unless otherwise stated. Statistical analyses were performed using Student's
925 t-tests (two-tailed). Where comparison of multiple groups was made either
926 one-way or two-way ANOVA with Bonferroni multiple comparisons was
927 performed. Differences with a p value of < 0.05 were considered significant.
928 Statistical significance for RNA seq was calculated using the QL F-test
929 followed by Benjamini-hochberg method of multiple testing correction.

930

931 **Miscellaneous:**

932 The molar extinction coefficient Per $[4Fe\text{-}4S]^{2+}$ cluster ($\varepsilon 413$
933 $=16200\ M^{-1}\ cm^{-1}$) was determined from *in vitro* reconstituted protein. Protein
934 concentration of SufR throughout the study was calculated using A_{280} reading.
935 Anti-SufR polyclonal antibody was used to monitor the expression and
936 purification of wt SufR and mutant proteins by Western blot. Samples (5 mg of

937 protein per slot) were resolved by 12% reducing SDS-PAGE and transferred
938 to nitrocellulose membrane. Blots were probed with primary and secondary
939 (horseradish peroxidase-conjugated anti- rabbit IgG) antibodies and
940 processed.

941

942 **Data availability:**

943 The RNA sequencing data presented in the manuscript are
944 deposited into the NCBI Gene Expression Omnibus (GEO)
945 (https://www.ncbi.nlm.nih.gov/geo/query/acc.cgi?acc=GSE154169 with the
946 accession number GSE154169 and reviewer token kbcdmqecrlotzgp.

947

948 **Author Disclosure Statement**

949 The funders had no role in study design, data collection and analysis,
950 decision to publish, or preparation of the manuscript. We confirm that no
951 competing financial interests exist.

952

953 **Acknowledgements:**

954 We are thankful to Next Generation Genomics Facility (NGGF) at
955 National Centre for Biological Sciences, Bangalore, for conducting the RNA
956 sequencing. We thank BSL3 facilities at CIDR, IISc Bangalore. We thank A.
957 Varalakshmi (Sophisticated Analytical Instrument Facility, IIT Chennai, India)
958 for excellent technical help In EPR experiments. The *Mtb* work was supported
959 by the following Wellcome Trust/DBT India Alliance Grants, IA/S/16/2/502700

(AS), IA/E/16/1/503017 (KA), and in part by Department of Biotechnology (DBT) Grant BT/PR11911/BRB/10/1327/2014, BT/PR5020/MED/29/1454/2012 (AS) and DBT-IISc Partnership Program (22-0905-0006-05-987-436). AS and KA are senior- and early- career fellows of Wellcome Trust/DBT India Alliance.

Author contributions:

KA, AT, and AS participated in the design of the study. KA, AT, KS, NM, AJ, RKJ, RSR, and, SNC, carried out the experiments. AR, VN, BG, GN, and ASN contributed to reagents and analyzed the data. KA and AS conceived the study, supervised the project, analyzed the data and drafted the manuscript. All authors read and approved the final manuscript.

Conflict of interest statement:

The authors have no conflict of interests to declare.

References

1. Mishra, B. B., Rathinam, V. A., Martens, G. W., Martinot, A. J., Kornfeld, H., Fitzgerald, K. A., and Sassetti, C. M. (2013) Nitric oxide controls the immunopathology of tuberculosis by inhibiting NLRP3 inflammasome-dependent processing of IL-1beta. *Nat Immunol* **14**, 52-60
2. Voskuil, M. I., Schnappinger, D., Visconti, K. C., Harrell, M. I., Dolganov, G. M., Sherman, D. R., and Schoolnik, G. K. (2003) Inhibition of respiration by nitric oxide induces a Mycobacterium tuberculosis dormancy program. *J Exp Med* **198**, 705-713
3. Nathan, C., and Shiloh, M. U. (2000) Reactive oxygen and nitrogen intermediates in the relationship between mammalian hosts and microbial pathogens. *Proc Natl Acad Sci U S A* **97**, 8841-8848

989 4. MacMicking, J., Xie, Q. W., and Nathan, C. (1997) Nitric oxide and
990 macrophage function. *Annual review of immunology* **15**, 323-350
991 5. MacMicking, J. D., North, R. J., LaCourse, R., Mudgett, J. S., Shah, S.
992 K., and Nathan, C. F. (1997) Identification of nitric oxide synthase as a
993 protective locus against tuberculosis. *Proc Natl Acad Sci U S A* **94**,
994 5243-5248
995 6. Nicholson, S., Bonecini-Almeida Mda, G., Lapa e Silva, J. R., Nathan,
996 C., Xie, Q. W., Mumford, R., Weidner, J. R., Calaycay, J., Geng, J.,
997 Boechat, N., Linhares, C., Rom, W., and Ho, J. L. (1996) Inducible
998 nitric oxide synthase in pulmonary alveolar macrophages from patients
999 with tuberculosis. *J Exp Med* **183**, 2293-2302
1000 7. Mattila, J. T., Ojo, O. O., Kepka-Lenhart, D., Marino, S., Kim, J. H.,
1001 Eum, S. Y., Via, L. E., Barry, C. E., 3rd, Klein, E., Kirschner, D. E.,
1002 Morris, S. M., Jr., Lin, P. L., and Flynn, J. L. (2013) Microenvironments
1003 in tuberculous granulomas are delineated by distinct populations of
1004 macrophage subsets and expression of nitric oxide synthase and
1005 arginase isoforms. *J Immunol* **191**, 773-784
1006 8. Wang, C. H., Liu, C. Y., Lin, H. C., Yu, C. T., Chung, K. F., and Kuo, H.
1007 P. (1998) Increased exhaled nitric oxide in active pulmonary
1008 tuberculosis due to inducible NO synthase upregulation in alveolar
1009 macrophages. *Eur Respir J* **11**, 809-815
1010 9. Schon, T., Elias, D., Moges, F., Melese, E., Tessema, T., Stendahl, O.,
1011 Britton, S., and Sundqvist, T. (2003) Arginine as an adjuvant to
1012 chemotherapy improves clinical outcome in active tuberculosis. *Eur*
1013 *Respir J* **21**, 483-488
1014 10. Schon, T., Idh, J., Westman, A., Elias, D., Abate, E., Diro, E., Moges,
1015 F., Kassu, A., Ayele, B., Forslund, T., Getachew, A., Britton, S.,
1016 Stendahl, O., and Sundqvist, T. (2011) Effects of a food supplement
1017 rich in arginine in patients with smear positive pulmonary tuberculosis--
1018 a randomised trial. *Tuberculosis (Edinb)* **91**, 370-377
1019 11. Kumar, A., Toledo, J. C., Patel, R. P., Lancaster, J. R., Jr., and Steyn,
1020 A. J. (2007) Mycobacterium tuberculosis DosS is a redox sensor and
1021 DosT is a hypoxia sensor. *Proc Natl Acad Sci U S A* **104**, 11568-11573
1022 12. Sardiwal, S., Kendall, S. L., Movahedzadeh, F., Rison, S. C., Stoker, N.
1023 G., and Djordjevic, S. (2005) A GAF domain in the hypoxia/NO-
1024 inducible Mycobacterium tuberculosis DosS protein binds haem. *J Mol*
1025 *Biol* **353**, 929-936
1026 13. Cortes, T., Schubert, O. T., Banaei-Esfahani, A., Collins, B. C.,
1027 Aebersold, R., and Young, D. B. (2017) Delayed effects of
1028 transcriptional responses in Mycobacterium tuberculosis exposed to
1029 nitric oxide suggest other mechanisms involved in survival. *Sci Rep* **7**,
1030 8208
1031 14. Shiloh, M. U., Manzanillo, P., and Cox, J. S. (2008) Mycobacterium
1032 tuberculosis senses host-derived carbon monoxide during macrophage
1033 infection. *Cell Host Microbe* **3**, 323-330
1034 15. Park, H. D., Guinn, K. M., Harrell, M. I., Liao, R., Voskuil, M. I., Tompa,
1035 M., Schoolnik, G. K., and Sherman, D. R. (2003) Rv3133c/dosR is a
1036 transcription factor that mediates the hypoxic response of
1037 Mycobacterium tuberculosis. *Mol Microbiol* **48**, 833-843

1038 16. Chinta, K. C., Saini, V., Glasgow, J. N., Mazorodze, J. H., Rahman, M.
1039 A., Reddy, D., Lancaster, J. R., Jr., and Steyn, A. J. (2016) The
1040 emerging role of gasotransmitters in the pathogenesis of tuberculosis.
1041 *Nitric Oxide* **59**, 28-41
1042 17. Huet, G., Daffe, M., and Saves, I. (2005) Identification of the
1043 Mycobacterium tuberculosis SUF machinery as the exclusive
1044 mycobacterial system of [Fe-S] cluster assembly: evidence for its
1045 implication in the pathogen's survival. *J Bacteriol* **187**, 6137-6146
1046 18. Singh, A., Guidry, L., Narasimhulu, K. V., Mai, D., Trombley, J.,
1047 Redding, K. E., Giles, G. I., Lancaster, J. R., Jr., and Steyn, A. J.
1048 (2007) Mycobacterium tuberculosis WhiB3 responds to O2 and nitric
1049 oxide via its [4Fe-4S] cluster and is essential for nutrient starvation
1050 survival. *Proc Natl Acad Sci U S A* **104**, 11562-11567
1051 19. Mehta, M., and Singh, A. (2019) Mycobacterium tuberculosis WhiB3
1052 maintains redox homeostasis and survival in response to reactive
1053 oxygen and nitrogen species. *Free Radic Biol Med* **131**, 50-58
1054 20. Kudhair, B. K., Hounslow, A. M., Rolfe, M. D., Crack, J. C., Hunt, D. M.,
1055 Buxton, R. S., Smith, L. J., Le Brun, N. E., Williamson, M. P., and
1056 Green, J. (2017) Structure of a Wbl protein and implications for NO
1057 sensing by M. tuberculosis. *Nature communications* **8**, 2280
1058 21. Hickok, J. R., Sahni, S., Shen, H., Arvind, A., Antoniou, C., Fung, L.
1059 W., and Thomas, D. D. (2011) Dinitrosyliron complexes are the most
1060 abundant nitric oxide-derived cellular adduct: biological parameters of
1061 assembly and disappearance. *Free Radic Biol Med* **51**, 1558-1566
1062 22. Fang, F. C. (2004) Antimicrobial reactive oxygen and nitrogen species:
1063 concepts and controversies. *Nat Rev Microbiol* **2**, 820-832
1064 23. Crack, J. C., Green, J., Thomson, A. J., and Le Brun, N. E. (2014) Iron-
1065 sulfur clusters as biological sensors: the chemistry of reactions with
1066 molecular oxygen and nitric oxide. *Acc Chem Res* **47**, 3196-3205
1067 24. Cook, G. M., Hards, K., Vilcheze, C., Hartman, T., and Berney, M.
1068 (2014) Energetics of Respiration and Oxidative Phosphorylation in
1069 Mycobacteria. *Microbiol Spectr* **2**
1070 25. Baughn, A. D., Garforth, S. J., Vilcheze, C., and Jacobs, W. R., Jr.
1071 (2009) An anaerobic-type alpha-ketoglutarate ferredoxin
1072 oxidoreductase completes the oxidative tricarboxylic acid cycle of
1073 Mycobacterium tuberculosis. *PLoS pathogens* **5**, e1000662
1074 26. Palde, P. B., Bhaskar, A., Pedro Rosa, L. E., Madoux, F., Chase, P.,
1075 Gupta, V., Spicer, T., Scampavia, L., Singh, A., and Carroll, K. S.
1076 (2016) First-in-Class Inhibitors of Sulfur Metabolism with Bactericidal
1077 Activity against Non-Replicating M. tuberculosis. *ACS chemical biology*
1078 **11**, 172-184
1079 27. Boshoff, H. I., Xu, X., Tahlan, K., Dowd, C. S., Pethe, K., Camacho, L.
1080 R., Park, T. H., Yun, C. S., Schnappinger, D., Ehrt, S., Williams, K. J.,
1081 and Barry, C. E., 3rd. (2008) Biosynthesis and recycling of
1082 nicotinamide cofactors in mycobacterium tuberculosis. An essential
1083 role for NAD in nonreplicating bacilli. *The Journal of biological*
1084 *chemistry* **283**, 19329-19341
1085 28. Buchko, G. W., Hewitt, S. N., Napuli, A. J., Van Voorhis, W. C., and
1086 Myler, P. J. (2011) Solution-state NMR structure and biophysical
1087 characterization of zinc-substituted rubredoxin B (Rv3250c) from

1088 Mycobacterium tuberculosis. *Acta Crystallogr Sect F Struct Biol Cryst*
1089 *Commun* **67**, 1148-1153
1090 29. Harper, A. E., Miller, R. H., and Block, K. P. (1984) Branched-chain
1091 amino acid metabolism. *Annu Rev Nutr* **4**, 409-454
1092 30. Munoz-Elias, E. J., and McKinney, J. D. (2006) Carbon metabolism of
1093 intracellular bacteria. *Cell Microbiol* **8**, 10-22
1094 31. Beites, T., O'Brien, K., Tiwari, D., Engelhart, C. A., Walters, S.,
1095 Andrews, J., Yang, H. J., Sutphen, M. L., Weiner, D. M., Dayao, E. K.,
1096 Zimmerman, M., Prideaux, B., Desai, P. V., Masquelin, T., Via, L. E.,
1097 Dartois, V., Boshoff, H. I., Barry, C. E., 3rd, Ehrt, S., and Schnappinger,
1098 D. (2019) Plasticity of the Mycobacterium tuberculosis respiratory chain
1099 and its impact on tuberculosis drug development. *Nature*
1100 *communications* **10**, 4970
1101 32. Brown, A. C., Eberl, M., Crick, D. C., Jomaa, H., and Parish, T. (2010)
1102 The nonmevalonate pathway of isoprenoid biosynthesis in
1103 Mycobacterium tuberculosis is essential and transcriptionally regulated
1104 by Dxs. *J Bacteriol* **192**, 2424-2433
1105 33. Ren, B., Zhang, N., Yang, J., and Ding, H. (2008) Nitric oxide-induced
1106 bacteriostasis and modification of iron-sulphur proteins in Escherichia
1107 coli. *Mol Microbiol* **70**, 953-964
1108 34. Tortora, V., Quijano, C., Freeman, B., Radi, R., and Castro, L. (2007)
1109 Mitochondrial aconitase reaction with nitric oxide, S-nitrosoglutathione,
1110 and peroxynitrite: mechanisms and relative contributions to aconitase
1111 inactivation. *Free Radic Biol Med* **42**, 1075-1088
1112 35. Lill, R. (2009) Function and biogenesis of iron-sulphur proteins. *Nature*
1113 **460**, 831-838
1114 36. Zhang, J., and Zhang, Q. (2019) Using Seahorse Machine to Measure
1115 OCR and ECAR in Cancer Cells. *Methods Mol Biol* **1928**, 353-363
1116 37. Dranka, B. P., Hill, B. G., and Darley-Usmar, V. M. (2010)
1117 Mitochondrial reserve capacity in endothelial cells: The impact of nitric
1118 oxide and reactive oxygen species. *Free Radic Biol Med* **48**, 905-914
1119 38. Bhaskar, A., Chawla, M., Mehta, M., Parikh, P., Chandra, P., Bhave,
1120 D., Kumar, D., Carroll, K. S., and Singh, A. (2014) Reengineering redox
1121 sensitive GFP to measure mycothiol redox potential of Mycobacterium
1122 tuberculosis during infection. *PLoS pathogens* **10**, e1003902
1123 39. Willemse, D., Weber, B., Masino, L., Warren, R. M., Adinolfi, S.,
1124 Pastore, A., and Williams, M. J. (2018) Rv1460, a SufR homologue, is
1125 a repressor of the suf operon in Mycobacterium tuberculosis. *PLoS*
1126 *One* **13**, e0200145
1127 40. Mishra, R., Kohli, S., Malhotra, N., Bandyopadhyay, P., Mehta, M.,
1128 Munshi, M., Adiga, V., Ahuja, V. K., Shandil, R. K., Rajmani, R. S.,
1129 Seshasayee, A. S. N., and Singh, A. (2019) Targeting redox
1130 heterogeneity to counteract drug tolerance in replicating
1131 Mycobacterium tuberculosis. *Sci Transl Med* **11**
1132 41. Li, Y., and He, Z. G. (2012) The mycobacterial LysR-type regulator
1133 OxyS responds to oxidative stress and negatively regulates expression
1134 of the catalase-peroxidase gene. *PLoS One* **7**, e30186
1135 42. Gomez, R. L., Jose, L., Ramachandran, R., Raghunandanan, S.,
1136 Muralikrishnan, B., Johnson, J. B., Sivakumar, K. C., Mundayoor, S.,
1137 and Kumar, R. A. (2016) The multiple stress responsive transcriptional

1138 regulator Rv3334 of Mycobacterium tuberculosis is an autorepressor
1139 and a positive regulator of kstR. *FEBS J* **283**, 3056-3071
1140 43. Smith, L. J., Stapleton, M. R., Fullstone, G. J., Crack, J. C., Thomson,
1141 A. J., Le Brun, N. E., Hunt, D. M., Harvey, E., Adinolfi, S., Buxton, R.
1142 S., and Green, J. (2010) Mycobacterium tuberculosis WhiB1 is an
1143 essential DNA-binding protein with a nitric oxide-sensitive iron-sulfur
1144 cluster. *The Biochemical journal* **432**, 417-427
1145 44. Leistikow, R. L., Morton, R. A., Bartek, I. L., Frimpong, I., Wagner, K.,
1146 and Voskuil, M. I. (2010) The Mycobacterium tuberculosis DosR
1147 regulon assists in metabolic homeostasis and enables rapid recovery
1148 from nonrespiring dormancy. *J Bacteriol* **192**, 1662-1670
1149 45. Tamuhla, T., Joubert, L., Willemse, D., and Williams, M. J. (2020) SufT
1150 is required for growth of Mycobacterium smegmatis under iron limiting
1151 conditions. *Microbiology* **166**, 296-305
1152 46. MacMicking, J. D., Taylor, G. A., and McKinney, J. D. (2003) Immune
1153 control of tuberculosis by IFN-gamma-inducible LRG-47. *Science* **302**,
1154 654-659
1155 47. Crack, J. C., den Hengst, C. D., Jakimowicz, P., Subramanian, S.,
1156 Johnson, M. K., Buttner, M. J., Thomson, A. J., and Le Brun, N. E.
1157 (2009) Characterization of [4Fe-4S]-containing and cluster-free forms
1158 of Streptomyces WhiD. *Biochemistry* **48**, 12252-12264
1159 48. Imlay, J. A. (2006) Iron-sulphur clusters and the problem with oxygen.
1160 *Mol Microbiol* **59**, 1073-1082
1161 49. Freibert, S. A., Weiler, B. D., Bill, E., Pierik, A. J., Muhlenhoff, U., and
1162 Lill, R. (2018) Biochemical Reconstitution and Spectroscopic Analysis
1163 of Iron-Sulfur Proteins. *Methods Enzymol* **599**, 197-226
1164 50. Cruz-Ramos, H., Crack, J., Wu, G., Hughes, M. N., Scott, C.,
1165 Thomson, A. J., Green, J., and Poole, R. K. (2002) NO sensing by
1166 FNR: regulation of the Escherichia coli NO-detoxifying
1167 flavohaemoglobin, Hmp. *EMBO J* **21**, 3235-3244
1168 51. Voskuil, M. I., Bartek, I. L., Visconti, K., and Schoolnik, G. K. (2011)
1169 The response of mycobacterium tuberculosis to reactive oxygen and
1170 nitrogen species. *Front Microbiol* **2**, 105
1171 52. Mishra, S., Shukla, P., Bhaskar, A., Anand, K., Baloni, P., Jha, R. K.,
1172 Mohan, A., Rajmani, R. S., Nagaraja, V., Chandra, N., and Singh, A.
1173 (2017) Efficacy of beta-lactam/beta-lactamase inhibitor combination is
1174 linked to WhiB4-mediated changes in redox physiology of
1175 Mycobacterium tuberculosis. *Elife* **6**
1176 53. Cortes, T., Schubert, O. T., Rose, G., Arnvig, K. B., Comas, I.,
1177 Aebersold, R., and Young, D. B. (2013) Genome-wide mapping of
1178 transcriptional start sites defines an extensive leaderless transcriptome
1179 in Mycobacterium tuberculosis. *Cell Rep* **5**, 1121-1131
1180 54. Mettert, E. L., and Kiley, P. J. (2015) How Is Fe-S Cluster Formation
1181 Regulated? *Annu Rev Microbiol* **69**, 505-526
1182 55. Cooper, C. E. (1999) Nitric oxide and iron proteins. *Biochim Biophys*
1183 *Acta* **1411**, 290-309
1184 56. Jones-Carson, J., Yahashiri, A., Kim, J. S., Liu, L., Fitzsimmons, L. F.,
1185 Weiss, D. S., and Vazquez-Torres, A. (2020) Nitric oxide disrupts
1186 bacterial cytokinesis by poisoning purine metabolism. *Sci Adv* **6**,
1187 eaaz0260

1188 57. Jones-Carson, J., Zweifel, A. E., Tapscott, T., Austin, C., Brown, J. M.,
1189 Jones, K. L., Voskuil, M. I., and Vazquez-Torres, A. (2014) Nitric oxide
1190 from IFNgamma-primed macrophages modulates the antimicrobial
1191 activity of beta-lactams against the intracellular pathogens Burkholderia
1192 pseudomallei and Nontyphoidal Salmonella. *PLoS Negl Trop Dis* **8**,
1193 e3079
1194 58. Jash, S., and Adhya, S. (2015) Effects of Transient Hypoxia versus
1195 Prolonged Hypoxia on Satellite Cell Proliferation and Differentiation In
1196 Vivo. *Stem Cells Int* **2015**, 961307
1197 59. Desler, C., Hansen, T. L., Frederiksen, J. B., Marcker, M. L., Singh, K.
1198 K., and Juel Rasmussen, L. (2012) Is There a Link between
1199 Mitochondrial Reserve Respiratory Capacity and Aging? *J Aging Res*
1200 **2012**, 192503
1201 60. Tyagi, P., Dharmaraja, A. T., Bhaskar, A., Chakrapani, H., and Singh,
1202 A. (2015) Mycobacterium tuberculosis has diminished capacity to
1203 counteract redox stress induced by elevated levels of endogenous
1204 superoxide. *Free Radic Biol Med* **84**, 344-354
1205 61. Kurthkoti, K., Amin, H., Marakalala, M. J., Ghanny, S., Subbian, S.,
1206 Sakatos, A., Livny, J., Fortune, S. M., Berney, M., and Rodriguez, G.
1207 M. (2017) The Capacity of Mycobacterium tuberculosis To Survive Iron
1208 Starvation Might Enable It To Persist in Iron-Deprived
1209 Microenvironments of Human Granulomas. *mBio* **8**
1210 62. Van den Bossche, A., Varet, H., Sury, A., Sismeiro, O., Legendre, R.,
1211 Coppee, J. Y., Mathys, V., and Ceyssens, P. J. (2019) Transcriptional
1212 profiling of a laboratory and clinical Mycobacterium tuberculosis strain
1213 suggests respiratory poisoning upon exposure to delamanid.
1214 *Tuberculosis (Edinb)* **117**, 18-23
1215 63. Kumar, M., Khan, F. G., Sharma, S., Kumar, R., Faujdar, J., Sharma,
1216 R., Chauhan, D. S., Singh, R., Magotra, S. K., and Khan, I. A. (2011)
1217 Identification of Mycobacterium tuberculosis genes preferentially
1218 expressed during human infection. *Microb Pathog* **50**, 31-38
1219 64. Pandey, M., Talwar, S., Bose, S., and Pandey, A. K. (2018) Iron
1220 homeostasis in Mycobacterium tuberculosis is essential for
1221 persistence. *Sci Rep* **8**, 17359
1222 65. Rybniker, J., Pojer, F., Marienhagen, J., Kolly, G. S., Chen, J. M., van
1223 Gumpel, E., Hartmann, P., and Cole, S. T. (2014) The cysteine
1224 desulfurase IscS of Mycobacterium tuberculosis is involved in iron-
1225 sulfur cluster biogenesis and oxidative stress defence. *The*
1226 *Biochemical journal* **459**, 467-478
1227 66. Gerrick, E. R., Barbier, T., Chase, M. R., Xu, R., Francois, J., Lin, V.
1228 H., Szucs, M. J., Rock, J. M., Ahmad, R., Tjaden, B., Livny, J., and
1229 Fortune, S. M. (2018) Small RNA profiling in Mycobacterium
1230 tuberculosis identifies MrsI as necessary for an anticipatory iron
1231 sparing response. *Proc Natl Acad Sci U S A* **115**, 6464-6469
1232 67. Li, H., and Durbin, R. (2009) Fast and accurate short read alignment
1233 with Burrows-Wheeler transform. *Bioinformatics* **25**, 1754-1760
1234 68. Li, H., Handsaker, B., Wysoker, A., Fennell, T., Ruan, J., Homer, N.,
1235 Marth, G., Abecasis, G., Durbin, R., and Genome Project Data
1236 Processing, S. (2009) The Sequence Alignment/Map format and
1237 SAMtools. *Bioinformatics* **25**, 2078-2079

1238 69. Quinlan, A. R., and Hall, I. M. (2010) BEDTools: a flexible suite of
1239 utilities for comparing genomic features. *Bioinformatics* **26**, 841-842
1240 70. Robinson, M. D., McCarthy, D. J., and Smyth, G. K. (2010) edgeR: a
1241 Bioconductor package for differential expression analysis of digital
1242 gene expression data. *Bioinformatics* **26**, 139-140
1243 71. Tian, J., Bryk, R., Itoh, M., Suematsu, M., and Nathan, C. (2005)
1244 Variant tricarboxylic acid cycle in Mycobacterium tuberculosis:
1245 identification of alpha-ketoglutarate decarboxylase. *Proc Natl Acad Sci*
1246 *U S A* **102**, 10670-10675
1247 72. Singh, A. K., Carette, X., Potluri, L. P., Sharp, J. D., Xu, R., Prisic, S.,
1248 and Husson, R. N. (2016) Investigating essential gene function in
1249 Mycobacterium tuberculosis using an efficient CRISPR interference
1250 system. *Nucleic Acids Res* **44**, e143
1251 73. Crack, J. C., Green, J., Thomson, A. J., and Le Brun, N. E. (2014)
1252 Techniques for the production, isolation, and analysis of iron-sulfur
1253 proteins. *Methods Mol Biol* **1122**, 33-48
1254 74. Maxam, A. M., and Gilbert, W. (1980) Sequencing end-labeled DNA
1255 with base-specific chemical cleavages. *Methods Enzymol* **65**, 499-560
1256
1257

1258
1259 **Figure legends (Main Figures):**
1260
1261 **Figure 1: Nitric oxide (NO) impacts Fe-S cluster transcriptome of *Mtb*.**
1262 Exponentially grown *Mtb* $H_{37}Rv$ was exposed to 0.5 mM DETA-NO for 4h in
1263 three biological replicates. Total RNA was isolated from untreated (UT) and
1264 DETA-NO treated (T) *Mtb* and subjected to RNA-seq analysis. Heat maps
1265 indicate $\log_2$ fold changes of differentially expressed genes (DEGs) belonging
1266 to various functional categories (obtained from Mycobrowser, EPFL,
1267 Lausanne). Genes were considered differentially expressed on the basis of
1268 the false discovery rate (FDR) of ≤0.05 and absolute fold change of ≥1.5.
1269 *BCCA: branched chain amino acid; BCKADH: branched chain keto-acid*
1270 *dehydrogenase complex*. *See also Figure 1-figure supplement 1 and Figure*
1271 *1-figure supplement 2.*

1272

1273 **Figure 2: NO affects Fe-S homeostasis and oxidative bioenergetics of**
1274 ***Mtb*. (A)** Gradual reduction of aconitase (Acn) activity in response to 0.5 mM
1275 DETA-NO over time. At 12 h post-treatment, *Mtb* was cultured in a DETA-NO
1276 free 7H9 broth for 24h and recovery (Rec) of Acn activity was quantified as a
1277 measure of Fe-S cluster regeneration. Under these conditions, intracellular
1278 levels of Acn remained unaltered. A non Fe-S cluster protein cystathione-β-
1279 synthase (Cbs) of *Mtb* was used as an internal loading control. **(B)** A change
1280 in Oxygen Consumption Rate (OCR) was quantified upon addition of indicated
1281 concentrations of DETA-NO by Seahorse XF flux analyzer. The uncoupler
1282 CCCP was used to maximally induce respiration and to determine the
1283 influence of NO on the spare respiratory capacity. The first and second

1284 vertical lines indicate the point of addition of DETA-NO and CCCP,
1285 respectively. **(C)** Extracellular Acidification Rate (ECAR) of DETA-NO treated
1286 *Mtb*. **(D)** Decrease in spare respiratory capacity of *Mtb* with increasing
1287 concentrations of DETA-NO. Percentage spare respiratory capacity was
1288 calculated by subtracting basal OCR (before adding DETA-NO) to CCCP
1289 induced OCR considering basal OCR as 100%. **(E)** *Mtb* expressing Mrx1-
1290 roGFP2 was exposed to the indicated concentrations of DETA-NO and
1291 changes in the biosensor ratio (405/488 nm) were measured using
1292 flowcytometer. **(F)** *Mtb* treated with the indicated concentrations of DETA-NO
1293 for 2 h was stained with CellRox Deep Red reagent to measure endogenous
1294 ROS. Results are expressed as Mean ± SD. One-way analysis of variance
1295 (ANOVA) with Bonferroni's post hoc test was employed to determine
1296 statistical significance between different doses of DETA-NO. Data shown are
1297 the result of three independent experiments performed in duplicate. *p* value is
1298 <0.05 were indicated with symbols. Symbols: (*): comparison to untreated *Mtb*
1299 control. Statistical significance for the OCR and ECAR was obtained by
1300 comparing different doses of DETA-NO with untreated (two-tailed, unpaired
1301 Student's t- test), Comparisons whose P value is <0.05 were indicated with
1302 different symbols. Symbols: (*): comparison to 0.25mM; (*): comparison to
1303 0.5mM; and (*): comparison to 1.0 mM. */*/* p<0.05; **/**/** p<0.01; ***/***/***
1304 p<0.001. ns, no significant difference (P > 0.05).

1305

1306 **Figure 3: SufR regulates Fe-S cluster biogenesis and DosR Regulon in**
1307 **response to NO.** Total RNA was isolated from three biological replicates of
1308 untreated (UT) and DETA-NO treated (T) *MtbΔsufR* and *sufR-Comp* and

1309 subjected to RNA-seq analysis. Heat maps indicate log2 fold changes of
1310 differentially expressed genes (DEGs) belonging to various functional
1311 categories (obtained from Mycobrowser, EPFL, Lausanne). Genes were
1312 considered differentially expressed on the basis of the false discovery rate
1313 (FDR) of ≤0.05 and absolute fold change of ≥1.5. "T" and "UT" indicate DETA-
1314 NO treated and untreated conditions, respectively. BCCA: branched chain
1315 amino acid. *See also Figure 3-figure supplement 1, Figure 3-figure*
1316 *supplement 2, and Figure 3-figure supplement 3.*

1317

1318 **Figure 4: SufR coordinates Fe-S cluster homeostasis, respiratory**
1319 **reserves, and redox balance in response to NO. (A)** Acn activity of
1320 *MtbΔsufR* in response to DETA-NO over time. At 12 h post-treatment,
1321 *MtbΔsufR* was cultured in a DETA-NO free 7H9 broth for 24h and recovery
1322 (Rec) of Acn activity was quantified as a measure of Fe-S cluster repair.
1323 Under these conditions, intracellular levels of Acn remained unaltered. A non
1324 Fe-S cluster protein cystathione-β-synthase (Cbs) was used as an internal
1325 loading control. **(B)** A change in OCR of *MtbΔsufR* was quantified upon
1326 addition of indicated concentrations of DETA-NO by Seahorse XF flux
1327 analyser. The uncoupler CCCP was used to maximally induce respiration and
1328 to determine the influence of NO on the spare respiratory capacity. The first
1329 and second vertical lines indicate point of addition of DETA-NO and CCCP,
1330 respectively. **(C)** Decrease in spare respiratory capacity of wt *Mtb* and
1331 *MtbΔsufR* with increasing concentrations of DETA-NO. **(D)** ECAR of DETA-
1332 NO-treated *MtbΔsufR.* **(E)** *Wt Mtb* and *MtbΔsufR* expressing Mrx1-roGFP2

1333 were exposed to the indicated concentrations of DETA-NO and changes in
1334 the biosensor ratio (405/488 nm) were measured using flowcytometry. **(F)** wt
1335 *Mtb* and *MtbΔsufR* treated with the indicated concentrations of DETA-NO for
1336 2 h was stained with CellRox Deep Red reagent to measure endogenous
1337 ROS. Data shown are the result of three independent experiments performed
1338 in triplicate (mean ± SD). One/two-way analysis of variance (ANOVA) as
1339 applicable with Bonferroni's post hoc test was employed to determine
1340 statistical significance between different doses of DETA-NO. *p* value is <0.05
1341 were indicated with symbols. Symbols: (*): comparison to untreated *Mtb*
1342 control, (#): comparision to untreated *MtbΔsufR*. Statistical significance for the
1343 OCR and ECAR was obtained by comparing different doses of DETA-NO with
1344 untreated (Two-tailed, unpaired Student's t- test.), Comparisons whose P
1345 value is <0.05 were indicated with different symbols. Symbols: (*): comparison
1346 to 0.25mM; (*): comparison to 0.5mM; and (*): comparison to 1.0 mM */*/*/#
1347 p<0.05; **/**/**/## p<0.01; ***/***/*** p<0.001. *See also Figure 4-figure*
1348 *supplement 1.*

1349

1350 **Figure 5: Fe-S cluster biogenesis enables recovery from NO-induced**
1351 **growth arrest *in vitro* and NO-dependent persistence in mice. (A)** Wt *Mtb*,
1352 *MtbΔsufR* and *sufR-Comp* were exposed to various doses of DETA-NO for
1353 24h and survival was monitored by enumerating CFUs. **(B)** Wt *Mtb*,
1354 *MtbΔsufR,* and *sufR-Comp* were either left untreated (UT) or treated (T) with
1355 repeated doses of 0.1 mM of DETA-NO for 36 h at an interval of 6 h and
1356 growth was monitored over time. **(C)** *Mtb* strains expressing CRISPRi vectors
1357 without (vector control) or with *sufT*-specific guide RNA (sgRNA) were left

1358 untreated (UT) or treated (T) with 0.1 mM of DETA-NO at an interval of 6 h for
1359 36 h and growth was monitored over time**.** To maintain reduced level of *sufT***,**
1360 anhydrotetracycline (ATc) 200 ng/ml was added for the induction of *sufT*
1361 specific–guide RNA and dCas9 every 48 h. A similar treatment of ATc was
1362 given to the control cells. **(D**) IFNγ-LPS-activated Raw264.7 cells were
1363 infected with wt *Mtb*, *MtbΔsufR* and *sufR -Comp* strains at moi 10 and
1364 intramacrophage survival was monitored by enumerating CFUS at the
1365 indicated time points. Data are the results of two independent experiments
1366 performed in triplicates. **(E)** Inbred BALB/c mice (*n* = 6) were given an aerosol
1367 challenge with wt *Mtb*, *MtbΔsufR* and *sufR-Comp* and assessed for survival in
1368 lungs at indicated time points. Results are expressed as mean ± standard
1369 deviation (SD). **(F)** C57BL/6 (n=5), **(G)** iNOS$^{-/-}$ knockout (n=5) mice were
1370 given an aerosol challenge with *wt Mtb* and *MtbΔsufR* and assessed for
1371 survival in lungs at indicated time points. Statistical significance for the
1372 intramacrophage and pulmonic load was obtained by comparing different
1373 strains, Comparisons whose *P* value is <0.05 were indicated with different
1374 symbols. Symbols: (*): comparison to wt *Mtb*; (#): comparison to *sufR-Comp*.
1375 */# p<0.05; **/## p<0.01; *** p<0.001. *See also Figure 5-figure supplement 1.*
1376
1377 **Figure 6: *Mtb* SufR is dimeric and coordinates 4Fe-4S cluster. (A)**
1378 Anaerobically-purified SufR was subjected to UV-visible spectroscopy. A clear
1379 peak at 413 nm indicates presence of a 4Fe-4S cluster. Addition of one
1380 electron reducing agent, dithionite (DTH; 5 mM) caused rapid bleaching of
1381 color and loss of the peak at 413 nm. Inset: **(i)** Ni^{2+}-NTA beads free of bound
1382 protein, **(ii)** dark brown colored Ni^{2+}-NTA beads due to binding of holo-SufR

1383 under anaerobic condition, and **(iii)** anaerobically purified holo-SufR exhibiting
1384 dark brown color. **(B)** Chromatographic profiles of apo- and holo-SufR eluting
1385 from a Superdex 200 HR gel filtration column. (Inset: standard curve
1386 generated from a linear fit of the log molecular weight of the protein standards
1387 versus their elution parameter V_e/V_o where, V_e is the elution volume and V_o is
1388 void volume). Both apo- and holo-SufR eluted at a volume corresponding to a
1389 molecular mass of ~54 kDa. **(C)** Holo-SufR and cysteine mutants of SufR (M1:
1390 C175A, M2: C175A_C179A; and M3: C175A_C179A_C192A) were purified
1391 anaerobically and scanned by a UV-vis spectrophotometer. The M2 and M3
1392 mutants of SufR showed absence of absorbance at 413 nm indicating loss of
1393 4Fe-4S cluster. **(D)** A far-UV CD spectrum of holo-SufR from 200 nm to 250
1394 nm wavelength. **(E)** Near-UV CD spectra of apo- and holo-SufR. **(F)** Chemical
1395 estimation of Fe and S content in holo-SufR. *See also Figure 6-figure*
1396 *supplement 1.*
1397
1398 **Figure 7: SufR responds to NO and H_2O_2 via 4Fe-4S cluster. (A)** UV-
1399 visible spectra were acquired before and after addition of proline NONOate
1400 (2.5 mM). A time dependent increase in the characteristic monomeric DNIC
1401 peak at ~ 350 nm was observed in the NO-treated sample. **(B)** Holo-SufR was
1402 exposed to various concentrations of proline NONOate (1, 5, and 10 -fold
1403 molar excess) and EPR spectra were acquired at a microwave frequency of
1404 9.667 GHz and microwave power of 2 mW at liquid nitrogen temperature. The
1405 peak at 2.025 *g* is consistent with the formation of monomeric DNIC. **(C)** Holo-
1406 sufR was exposed to atmospheric O_2 by bubbling air through the sample for 2
1407 min. UV-visible spectra were acquired before and after exposure at various

1408 time intervals as indicated. **(D)** Holo-SufR was treated with a fixed
1409 concentration of H_2O_2 (1 mM) and absorbance was monitored over time. The
1410 gradual decrease in absorbance around 413 nm indicates loss of Fe-S
1411 cluster. (Inset **C, D**) Rate of the 4Fe-4S cluster loss was determined by
1412 calculating the percent loss of absorbance at 413 nm upon exposure to air
1413 and H_2O_2 at various time intervals. *See also Figure 7-figure supplement 1.*
1414
1415 **Figure 8: DNA binding activity of holo-SufR is dependent on NO and**
1416 **H_2O_2. (A)** EMSA of holo- and apo-SufR binding to ^{32}P-labelled *suf* promoter
1417 DNA fragment (0.5 nM). The concentrations of holo- and apo-SufR used for
1418 EMSAs were 0.125 μM, 0.25 μM, 0.5 μM, 1 μM, and 2 μM. Holo SufR (0.5
1419 μM) was pretreated with **(B)** proline NONOate (NO; 2.5-, 5-, and 10-fold molar
1420 excess) or **(C)** H_2O_2 (25, 50, 75, 100, 250, 500, 1000 and 5000 nM) and were
1421 incubated with ^{32}P-labelled *suf* promoter. **(D)** Holo SufR (0.5 μM) was
1422 incubated with ^{32}P-labelled *suf* promoter and DNA binding was competed out
1423 using 12.5-, 25-, 50-, and 100-fold molar excess of unlabelled competitor
1424 promoter fragment of *suf* operon and *blaC.* **(E)** Effect of holo- and apo-SufR
1425 on transcription from *suf* promoter *in vitro*. Single-round transcription assays
1426 show that RNAP-σA efficiently directs transcription from the *suf* promoter
1427 giving an expected product of 107 bp. Increasing concentrations of holo-SufR
1428 inhibit transcription. **(F)** Apo-SufR was completely ineffective in inhibiting
1429 transcription. **(G)** Holo SufR (0.25 μM) pre-treated with proline NONOate (NO;
1430 2.5-, and 5 -fold molar excess) stimulated transcription in a dose dependent
1431 manner. The graph below indicates densitometry analysis of the *suf* transcript
1432 (*n*=2). One-way analysis of variance (ANOVA) with Bonferroni's post hoc test

1433 was employed to determine statistical significance. Statistical significance was
1434 obtained by comparing with SufR untreated. '*' $p<0.05$ '**' $p<0.01$ '***'
1435 $p<0.001$. See also Figure 8-figure supplement 1.
1436
1437 **Figure 9: DNase I footprint of holo-SufR bound to the *suf* promoter.**
1438 Sequence upstream of the *suf* operon (KA10t and its complementary strand-
1439 KA11t) were used for DNase I footprint. Bold letter **G** in the sequence is the
1440 transcription start site (TSS) as well start codon for *Mtb* SufR**. (A)** KA10t was
1441 labeled with ^{32}P and annealed with cold KA11t. **(B)** KA11t was labeled with
1442 ^{32}P and annealed with cold KA10 in order to examine the protected region in
1443 the reverse strand. Reactions containing 5 nM ^{32}P-labeled dsDNA substrate
1444 were incubated either in absence or in the presence of increasing
1445 concentration of purified holo-SufR protein (125 nM, 250 nM, 500 nM, 1 μM,).
1446 0.05 U of DNase I was added to the reaction mixture and digestion was
1447 carried out for 2 mins at room temperature. A+G is Maxam and Gilbert
1448 sequencing ladder. DNase I protected nucleotides are marked with red and
1449 two inverted repeats are marked by arrow (blue and black). **(C-E)** EMSA was
1450 performed with wild type (KA10t and KA11t) and oligonucleotides with
1451 mutations in the inverted repeats (KA10tm1, KA11tm1, KA10tm2 and
1452 KA11tm2) at increasing concentrations of NaCl at two different concentrations
1453 of SufR (0.25 μM and 0.5 μM).
1454
1455 **Figure 10: A model for SufR-mediated regulation of Fe-S cluster**
1456 **biogenesis in *Mtb*.** SufR appears to coordinate the expression of the *suf*
1457 operon in a negative feedback loop. Under Fe sufficient conditions, the Fe-S

1458 cluster bound form of SufR (holo-SufR) binds to the promoter of the *suf*
1459 operon and represses Fe-S biogenesis. Exposure to NO or H_2O_2 damages
1460 Fe-S clusters to generate DNIC or apo-forms of SufR, respectively, which
1461 abrogates SufR DNA binding resulting in de-repression of the *suf* operon. The
1462 elevated expression of the SUF Fe-S assembly system regenerates Fe-S
1463 clusters of metabolic enzymes, respiratory complexes, and redox sensors to
1464 maintain Fe-S homeostasis, spare respiratory capacity, and redox balance.
1465 The NO sensing properties of SufR via its 4Fe-4S cluster and persistence
1466 defect exhibited by *MtbΔsufR* in mice in an iNOS-dependent manner suggest
1467 that SufR integrates host environmental signals to Fe-S cluster homeostasis
1468 in *Mtb*.
1469

1470 **Figure Supplement Legends**

1471 **Figure 1-figure supplement 1: NO arrests growth of *Mtb***: *Mtb* strain was
1472 treated with slow release NO donor DETA-NO (0.5 mM) and growth were
1473 monitored by enumerating CFU at the indicated time points. Data shown are
1474 the result of three independent experiments performed in duplicate. Results
1475 are expressed as (Mean±SD). One-way analysis of variance (ANOVA) with
1476 Bonferroni's post hoc test was employed to determine statistical significance.
1477 Statistical significance was obtained by comparing untreated and treated at
1478 different time point with untreated control (0h). '*' $p<0.05$. '***' $p<0.001$.

1479

1480 **Figure 1-figure supplement 2: Regulation of multiple pathways and**
1481 **regulons upon NO stress in *Mtb*.** Exponentially grown wt *Mtb was* exposed

1482 to 500 μM DETA-NO for 4h. Total RNA was isolated and subjected to RNA-
1483 seq analysis. Heat maps depicting expression of genes (log_2fold-change≥1;
1484 FDR≤0.05) coordinating dormancy regulon, Fe- homeostasis, Zn-
1485 homeostasis, Cu- homeostasis, transcription and translation, Redox
1486 homeostasis, DNA repair, and central carbon metabolism for untreated (UT)
1487 and 4 hr of DETA-NO-treated (T) *Mtb* from three biological samples.

1488

1489 **Figure 3-figure supplement 1: NO arrests growth of *wt Mtb*, *MtbΔsufR***
1490 **and *sufR–Comp***. *Mtb* strains were treated with DETA-NO (0.5 mM) and
1491 survival was monitored by enumerating CFU at the indicated time points. Data
1492 shown are the result of three independent experiments performed in
1493 duplicate. Results are expressed as (Mean±SD).

1494

1495 **Figure 3-figure supplement 2: Impact of SufR on the transcriptome of**
1496 ***Mtb* in response to NO.** *wt Mtb*, *MtbΔsufR* and *sufR-Comp* strains were
1497 grown and exposed to 500 μM DETA-NO for 4h. Total RNA was isolated from
1498 three biological replicates and subjected to RNA-seq analysis. Heat maps
1499 depicting expression of various pathways (log_2fold-change≥1; FDR≤0.05)
1500 between DETA-NO-treated (T) and untreated conditions.

1501

1502 **Figure 3-figure supplement 3: Genomic organization of *sufR***: **(A)** 5'RACE
1503 confirmed the presence of two TSS (transcription start site) for the *suf* operon.
1504 Primary TSS1 upstream of *sufR* (*Rv1460*) is marked in blue and alternate

1505 TSS2 upstream of *sufB* (*Rv1461*) marked in violet. Nucleotide position was
1506 marked according to mycobrowser and NCBI. Genomic region deleted in
1507 *MtbΔsufR* is marked as red and intact region is marked as green. **(B)** RNA-
1508 seq data showing the expression of undeleted region of *sufR* in response to
1509 NO in wt *Mtb*, *MtbΔsufR*, and *sufR-Comp*.

1510

1511 **Figure 4-figure supplement 1: Aconitase activity of *sufR-Comp* strain**
1512 **upon NO stress.** Upon exposure to 0.5 mM DETA-NO, Aconitase (Acn)
1513 activity in *sufR-Comp* was decreased in a time dependent manner similar to
1514 *Mtb* and *MtbΔsufR*. After 12h of NO stress, cells were freshly cultured in NO-
1515 free 7H9 broth for 24h and subjected to Acn activity. No recovery in Acn
1516 activity was observed after 24h. The change in enzymatic activity is
1517 independent of Acn abundance. Data shown are the result of three
1518 independent experiments. Results are expressed as (Mean±SD). One-way
1519 analysis of variance (ANOVA) with Bonferroni's post hoc test was employed to
1520 determine statistical significance. Statistical significance was obtained by
1521 comparing DETA-NO treated at different time point with untreated control
1522 (0h). '*' $p<0.05$. '***' $p<0.001$.

1523

1524 **Figure 5-figure supplement 1: Histopathology of BALB/C lungs infected**
1525 **with *Mtb*, *MtbΔsufR* and *ΔsufR-Comp*. A)** Representative H&E staining of
1526 the lung tissue sections of BALB/c mice eight weeks' post infection. **B)** Scatter
1527 plots indicate modified granuloma score for lung section histopathology of
1528 chronically-infected BALB/c mice across experimental groups at eight weeks

1529 post-infection. Results are expressed as (median±inter-quartile range). '*'
1530 $p<0.05$. '***' $p<0.001$. One-way analysis of variance (ANOVA) with
1531 Bonferroni's post hoc test was employed to determine statistical significance.
1532 Statistical significance was obtained by comparing with *Mtb*. (n=4)

1533

1534 **Figure 6-figure supplement 1: Purification and spectroscopic**
1535 **characterization of *Mtb* SufR (Rv1460): (A)** UV- visible spectra of *Mtb* SufR
1536 purified under aerobic and anaerobic condition **(B)** UV- visible absorption
1537 spectrum of *Mtb* SufR purified in native condition shows the presence of 4Fe-
1538 4S cluster indicated by arrow (λmax- 413 nm). Presence of broad peaks at
1539 410-420 nm indicates the presence of a [4Fe-4S] cluster in SufR (Holo-SufR).
1540 **(C)** SDS-PAGE confirming the purification of SufR (27.5 kDa). I: Induced, UI:
1541 Un-induced, W1, W2, W3: Wash through fractions, M: Protein marker, E1, E2,
1542 and E3: Elution fractions.

1543

1544 **Figure 7-figure supplement 1: *4Fe-4S cluster of* SufR is sensitive to**
1545 **H_2O_2.** Holo SufR was treated either with the **(A)** indicated concentrations of
1546 H_2O_2 for 1 min or a fixed concentration of H_2O_2 **(B)** 10 mM **(C)** 0.1 mM and
1547 absorbance was monitored over time. The gradual decrease in absorbance at
1548 413 nm indicates loss of Fe-S cluster. **(**Inset **C)** Rate of the 4Fe-4S cluster
1549 loss was determined by calculating the percent loss of absorbance at 413 nm
1550 upon exposure to H_2O_2 at various time intervals.

1551

1552 **Figure 8-figure supplement 1: CRISPRi of *sufT* in *Mtb***. Expression of *sufT*
1553 along with *sufR, sufB, sufD, sufC, sufS,* and *sufU* in SufT knock-down (KD)
1554 strain added with ATC (Induced) for 24 h, with respect to control strain not
1555 added with ATC (without induction). The significance of the difference in
1556 gene-specific RNA between samples from induced and uninduced cultures is
1557 indicated by asterisks above the bar for the induced sample (*$P < 0.05$; **$P <$
1558 0.001; ***$P < 0.0001$). Data shown are the result of three independent
1559 experiments performed in duplicate. Results are expressed as (Mean±SD).
1560

1561 **<u>List of figure supplements:</u>**

1562 **Figure 1-figure supplement 1:** NO arrests growth of *Mtb*.

1563 **Figure 1-figure supplement 2:** Regulation of multiple pathways and regulons
1564 upon NO stress in *Mtb*.

1565 **Figure 3-figure supplement 1:** NO arrests growth of wt *Mtb*, *MtbΔsufR* and
1566 *sufR–Comp*.

1567 **Figure 3-figure supplement 2:** Impact of SufR on the transcriptome of *Mtb* in
1568 response to NO.

1569 **Figure 3-figure supplement 3:** Genomic organization of *sufR*.

1570 **Figure 4-figure supplement 1:** Aconitase activity of *sufR-Comp* strain upon
1571 NO stress.

1572 **Figure 5-figure supplement 1:** Histopathology of BALB/C lungs infected with

1573 **Figure 6-figure supplement 1:** Purification and spectroscopic
1574 characterization of *Mtb* SufR (Rv1460).

1575 **Figure 7-figure supplement 1:** 4Fe-4S cluster of SufR is sensitive to H_2O_2.

1576 **Figure 8-figure supplement 1:** CRISPRi of *sufT* in *Mtb*.

1577

1578 **List of Supplementary files:**

1579 **Supplementary file 1A:** Differentially regulated genes in *wt Mtb* upon
1580 exposure to 0.5mM DETA-NO as compare to untreated *wt Mtb* [$\log_2$fold-
1581 change≥1; FDR≤0.05]. (Enclosed as a separate excel spread sheet).

1582

1583 **Supplementary file 1B:** List of Fe-S cluster protein differentially regulated in
1584 DETA-NO treated *wt Mtb* as compared to untreated wt *Mtb*. [fold change ≥
1585 1.5; FDR ≤ 0.05] (Enclosed as a separate excel spread sheet).

1586

1587 **Supplementary file 1C:** Genes differentially regulated in DETA-NO treated
1588 *MtbΔsufR* as compared to untreated *MtbΔsufR* [$\log_2$ fold-change≥1;
1589 FDR≤0.05]. (Enclosed as a separate excel spread sheet).

1590

1591 **Supplementary file 1D:** Genes differentially regulated in DETA-NO treated
1592 *MtbΔsufR* as compared to DETA-NO treated *wt Mtb*, DETA-NO treated *sufR-*
1593 *Comp* as compared to DETA-NO treated *wt Mtb*, and DETA-NO treated *sufR-*
1594 *Comp* as compared to DETA-NO treated *wt MtbΔsufR* [fold change ≥ 1.5;
1595 FDR ≤ 0.05]. (Enclosed as a separate excel spread sheet).

1596

1597 **Supplementary file 2:** List of genes differentially regulated in DETA-NO
1598 treated *MtbΔsufR* as compared to DETA-NO treated *wt Mtb* [fold change ≥
1599 1.5; FDR ≤ 0.05]) having similar *sufR* binding motifs as identified using
1600 DNAase I footprint (Figure 9).

1601

1602 **Supplementary file 3**: Sequences of primers used in this study.

Figure 1

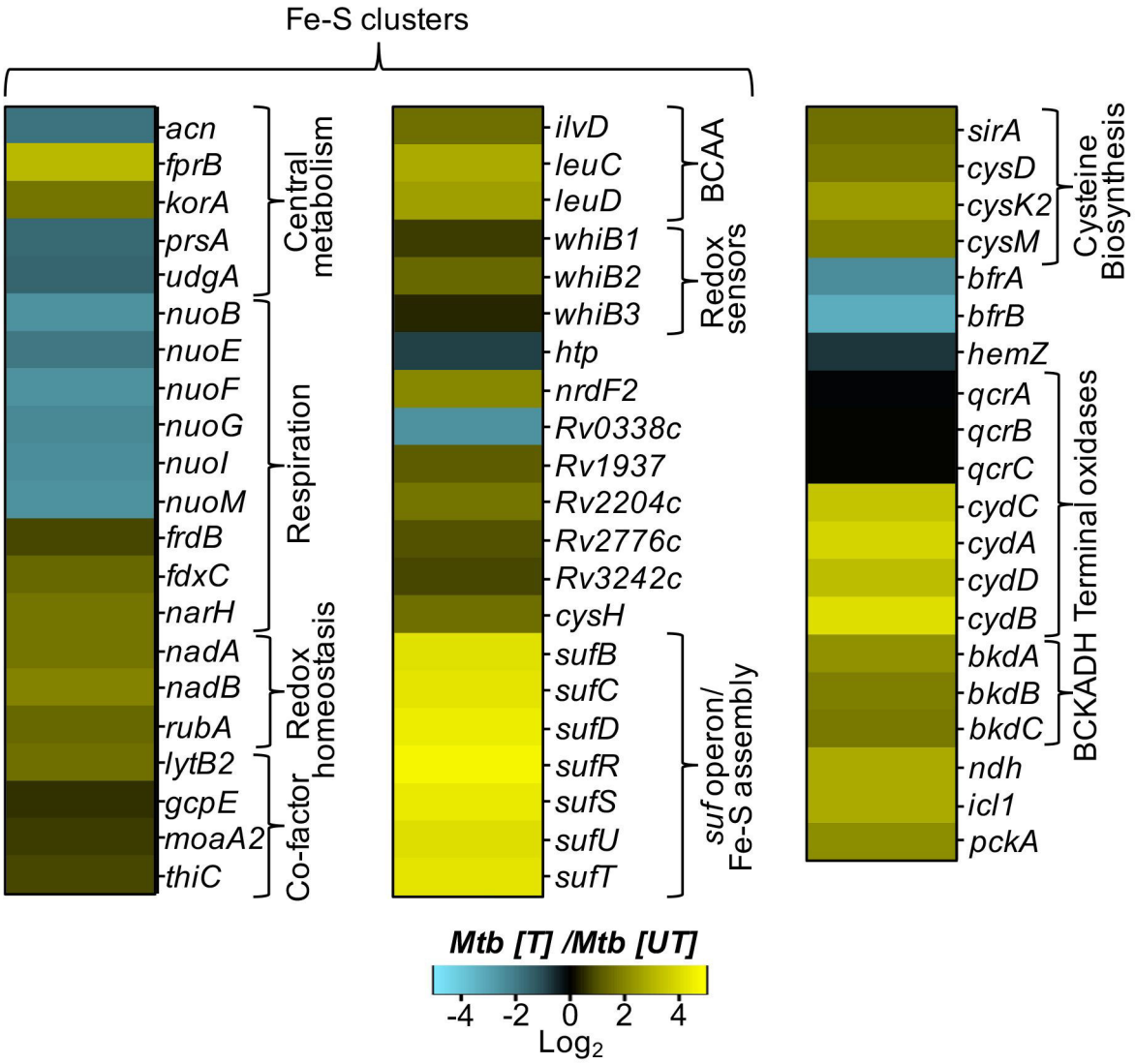
Fe-S clusters
acn
fprB
korA
prsA
udgA
nuoB
nuoE
nuoF
nuoG
nuoI
nuoM
frdB
fdxC
narH
nadA
nadB
rubA
lytB2
gcpE
moaA2
thiC
Central metabolism
Respiration
Redox homeostasis
Co-factor
ilvD
leuC
leuD
whiB1
whiB2
whiB3
htp
nrdF2
Rv0338c
Rv1937
Rv2204c
Rv2776c
Rv3242c
cysH
sufB
sufC
sufD
sufR
sufS
sufU
sufT
BCAA
Redox sensors
suf operon/ Fe-S assembly
sirA
cysD
cysK2
cysM
bfrA
bfrB
hemZ
qcrA
qcrB
qcrC
cydC
cydA
cydD
cydB
bkdA
bkdB
bkdC
ndh
icl1
pckA
Cysteine Biosynthesis
Terminal oxidases
BCKADH
Mtb [T] /Mtb [UT]
-4
-2
0
2
4
Log2

Figure 2

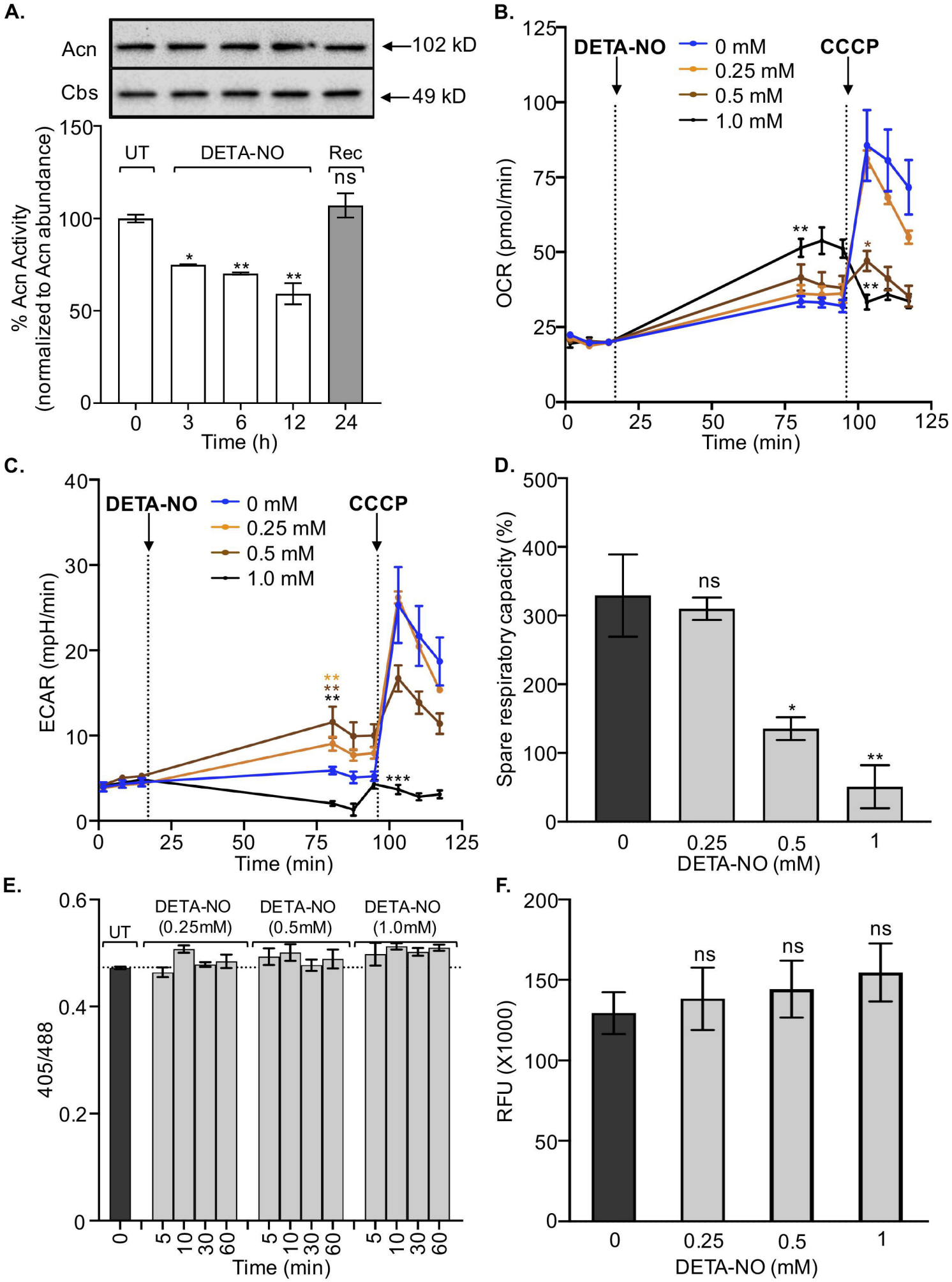
A.
Acn
Cbs
102 kD
49 kD
% Acn Activity
(normalized to Acn abundance)
UT
DETA-NO
Rec
ns
Time (h)
B.
DETA-NO
CCCP
0 mM
0.25 mM
0.5 mM
1.0 mM
OCR (pmol/min)
Time (min)
C.
DETA-NO
CCCP
0 mM
0.25 mM
0.5 mM
1.0 mM
ECAR (mpH/min)
Time (min)
D.
Spare respiratory capacity (%)
ns
DETA-NO (mM)
E.
UT
DETA-NO (0.25mM)
DETA-NO (0.5mM)
DETA-NO (1.0mM)
405/488
Time (min)
F.
RFU (X1000)
ns
DETA-NO (mM)

Figure 3

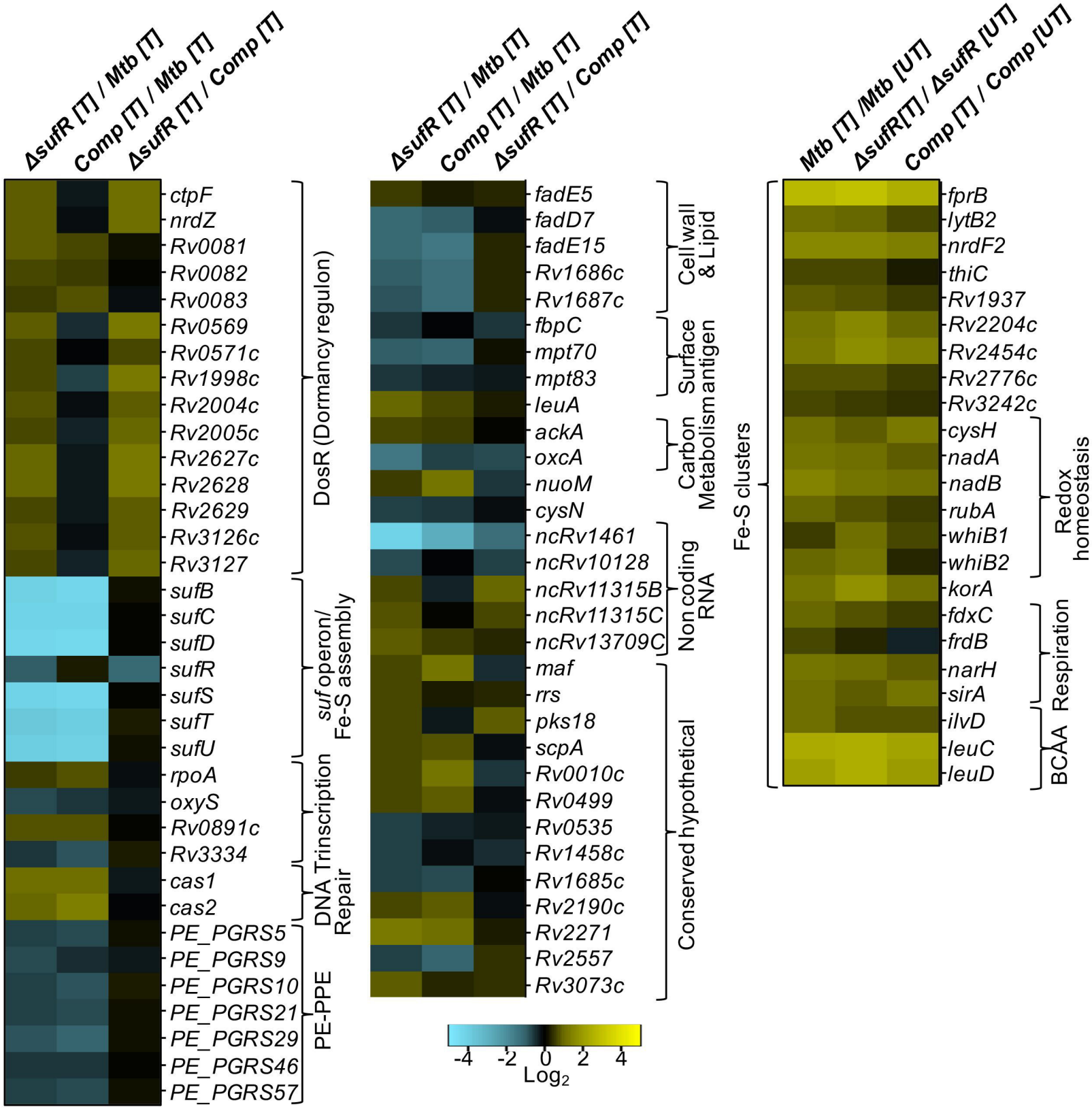
ΔsufR [T] / Mtb [T]
Comp [T] / Mtb [T]
ΔsufR [T] / Comp [T]
ctpF
nrdZ
Rv0081
Rv0082
Rv0083
Rv0569
Rv0571c
Rv1998c
Rv2004c
Rv2005c
Rv2627c
Rv2628
Rv2629
Rv3126c
Rv3127
sufB
sufC
sufD
sufR
sufS
sufT
sufU
rpoA
oxyS
Rv0891c
Rv3334
cas1
cas2
PE_PGRS5
PE_PGRS9
PE_PGRS10
PE_PGRS21
PE_PGRS29
PE_PGRS46
PE_PGRS57
DosR (Dormancy regulon)
suf operon/ Fe-S assembly
Trinscription
DNA Repair
PE-PPE
ΔsufR [T] / Mtb [T]
Comp [T] / Mtb [T]
ΔsufR [T] / Comp [T]
fadE5
fadD7
fadE15
Rv1686c
Rv1687c
fbpC
mpt70
mpt83
leuA
ackA
oxcA
nuoM
cysN
ncRv1461
ncRv10128
ncRv11315B
ncRv11315C
ncRv13709C
maf
rrs
pks18
scpA
Rv0010c
Rv0499
Rv0535
Rv1458c
Rv1685c
Rv2190c
Rv2271
Rv2557
Rv3073c
Cell wall & Lipid
Surface antigen
Carbon Metabolism
Non coding RNA
Conserved hypothetical
-4
-2
0
2
4
Log2
Mtb [T] /Mtb [UT]
ΔsufR[T] / ΔsufR [UT]
Comp [T] / Comp [UT]
fprB
lytB2
nrdF2
thiC
Rv1937
Rv2204c
Rv2454c
Rv2776c
Rv3242c
cysH
nadA
nadB
rubA
whiB1
whiB2
korA
fdxC
frdB
narH
sirA
ilvD
leuC
leuD
Fe-S clusters
Redox homeostasis
Respiration
BCAA

Figure 4

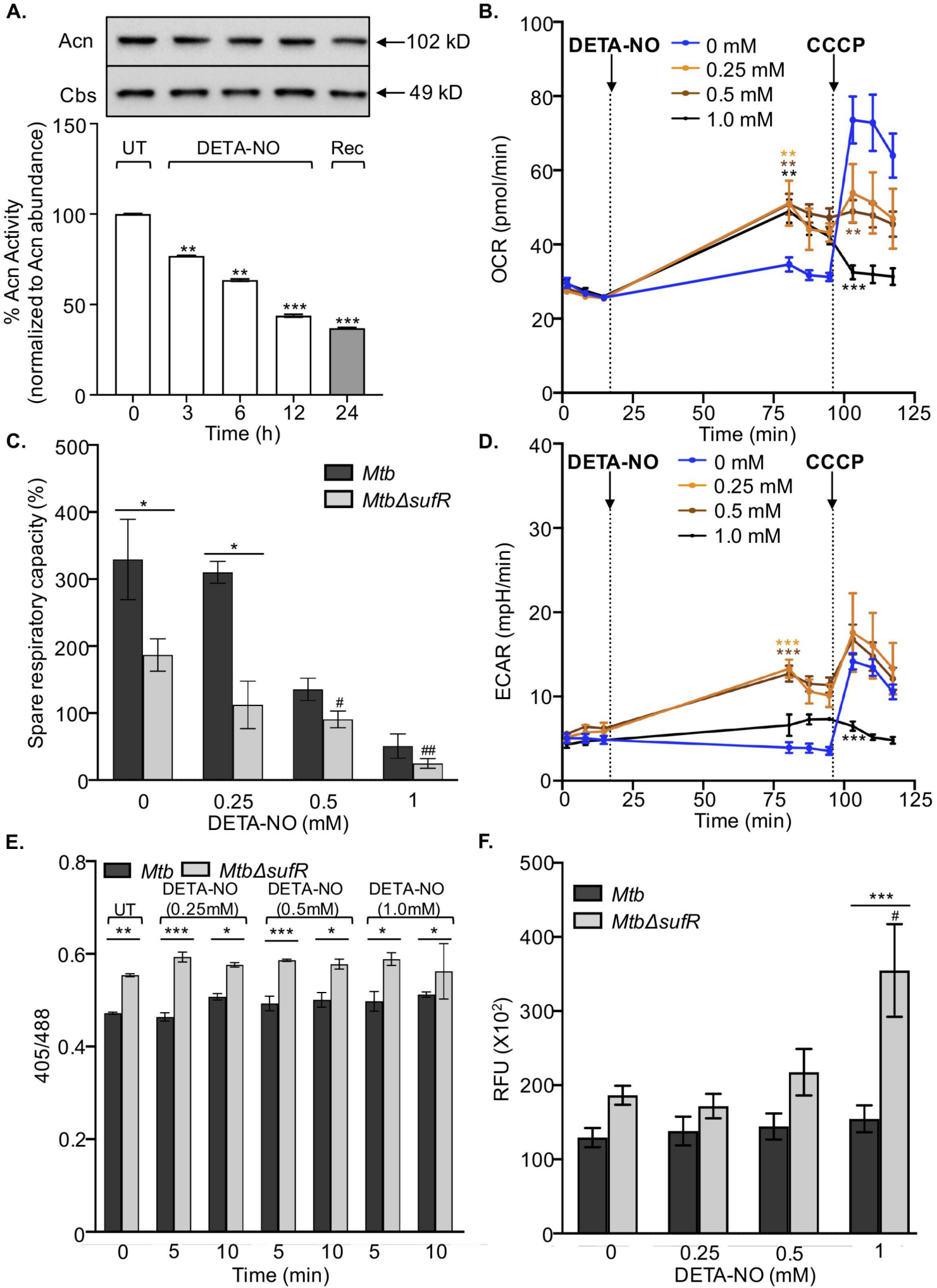
A.
Acn
Cbs
102 kD
49 kD
UT
DETA-NO
Rec
% Acn Activity
(normalized to Acn abundance)
Time (h)
B.
DETA-NO
CCCP
0 mM
0.25 mM
0.5 mM
1.0 mM
OCR (pmol/min)
Time (min)
C.
Mtb
MtbΔsufR
Spare respiratory capacity (%)
DETA-NO (mM)
D.
ECAR (mpH/min)
E.
405/488
DETA-NO (0.25mM)
DETA-NO (0.5mM)
DETA-NO (1.0mM)
F.
RFU (X10²)

Figure 5

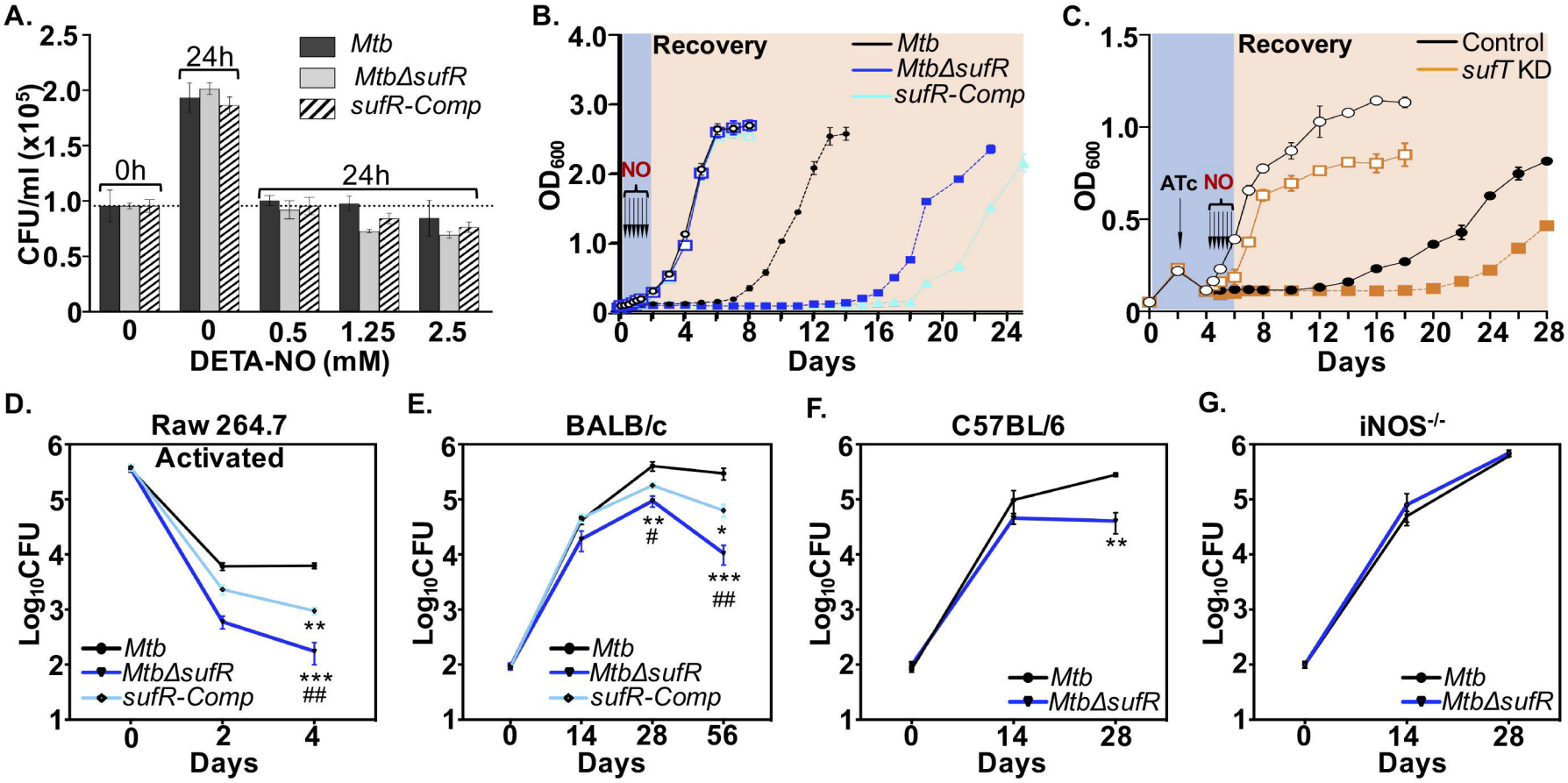
A.
CFU/ml (x10^5)
0h
24h
24h
Mtb
MtbΔsufR
sufR-Comp
DETA-NO (mM)
B.
Recovery
NO
Mtb
MtbΔsufR
sufR-Comp
OD600
Days
C.
Recovery
ATc
NO
Control
sufT KD
OD600
Days
D.
Raw 264.7
Activated
Log10CFU
Mtb
MtbΔsufR
sufR-Comp
Days
E.
BALB/c
Log10CFU
Mtb
MtbΔsufR
sufR-Comp
Days
F.
C57BL/6
Log10CFU
Mtb
MtbΔsufR
Days
G.
iNOS-/-
Log10CFU
Mtb
MtbΔsufR
Days

Figure 6

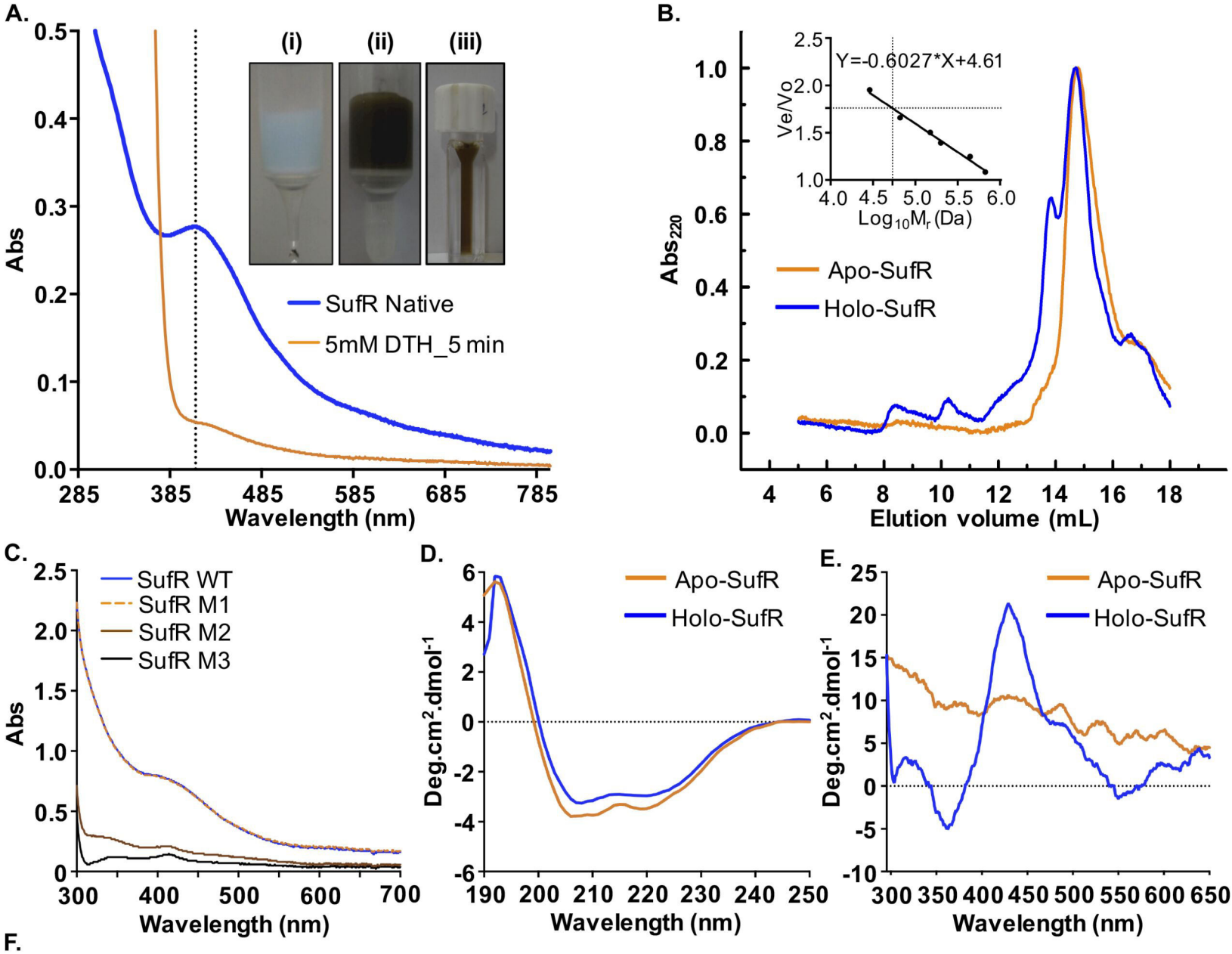

F.

Chemical assay of non-heme iron and acid-labile sulfide of holo-SufR				
	Batch 1	Batch 2	Batch 3	Average
Iron (μM)	300.29±32[b]	295.88±11[c]	259.12±25[d]	291.76±29.27
Sulfide (μM)	287.36±40[b]	286.71±28[b]	277.36±76[d]	285.11±38.46
Protein (μM)	80	80	80	80
Iron/Protein[a]	3.75±0.4	3.7±0.14	3.23±0.32	3.64±0.4
Sulfide/protein[a]	3.59±0.5	3.58±0.35	3.47±0.95	3.54±0.5
Fe:S	1.05±0.08	1.08±0.09	0.95±0.17	1.03±0.1

[a] With reference to the monomer of SufR
[b] Average of four
[c] Average of three
[d] Average of two

Figure 7

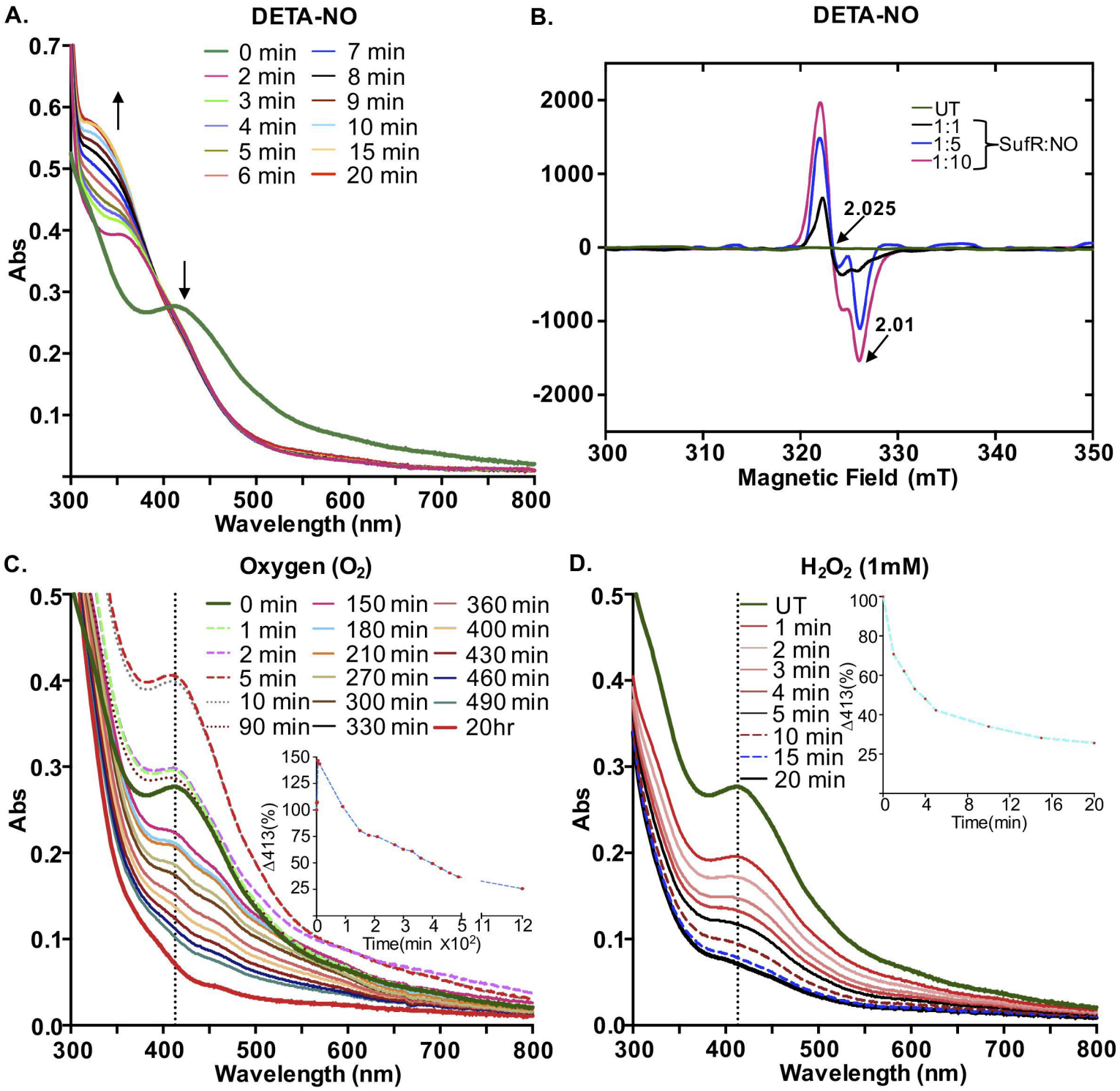
A.
DETA-NO
0 min
2 min
3 min
4 min
5 min
6 min
7 min
8 min
9 min
10 min
15 min
20 min
Abs
Wavelength (nm)
B.
DETA-NO
UT
1:1
1:5
1:10
SufR:NO
2.025
2.01
Magnetic Field (mT)
C.
Oxygen (O_2)
0 min
1 min
2 min
5 min
10 min
90 min
150 min
180 min
210 min
270 min
300 min
330 min
360 min
400 min
430 min
460 min
490 min
20hr
Δ413(%)
Time(min X10²)
Abs
Wavelength (nm)
D.
H_2O_2 (1mM)
UT
1 min
2 min
3 min
4 min
5 min
10 min
15 min
20 min
Δ413(%)
Time(min)
Abs
Wavelength (nm)

Figure 9

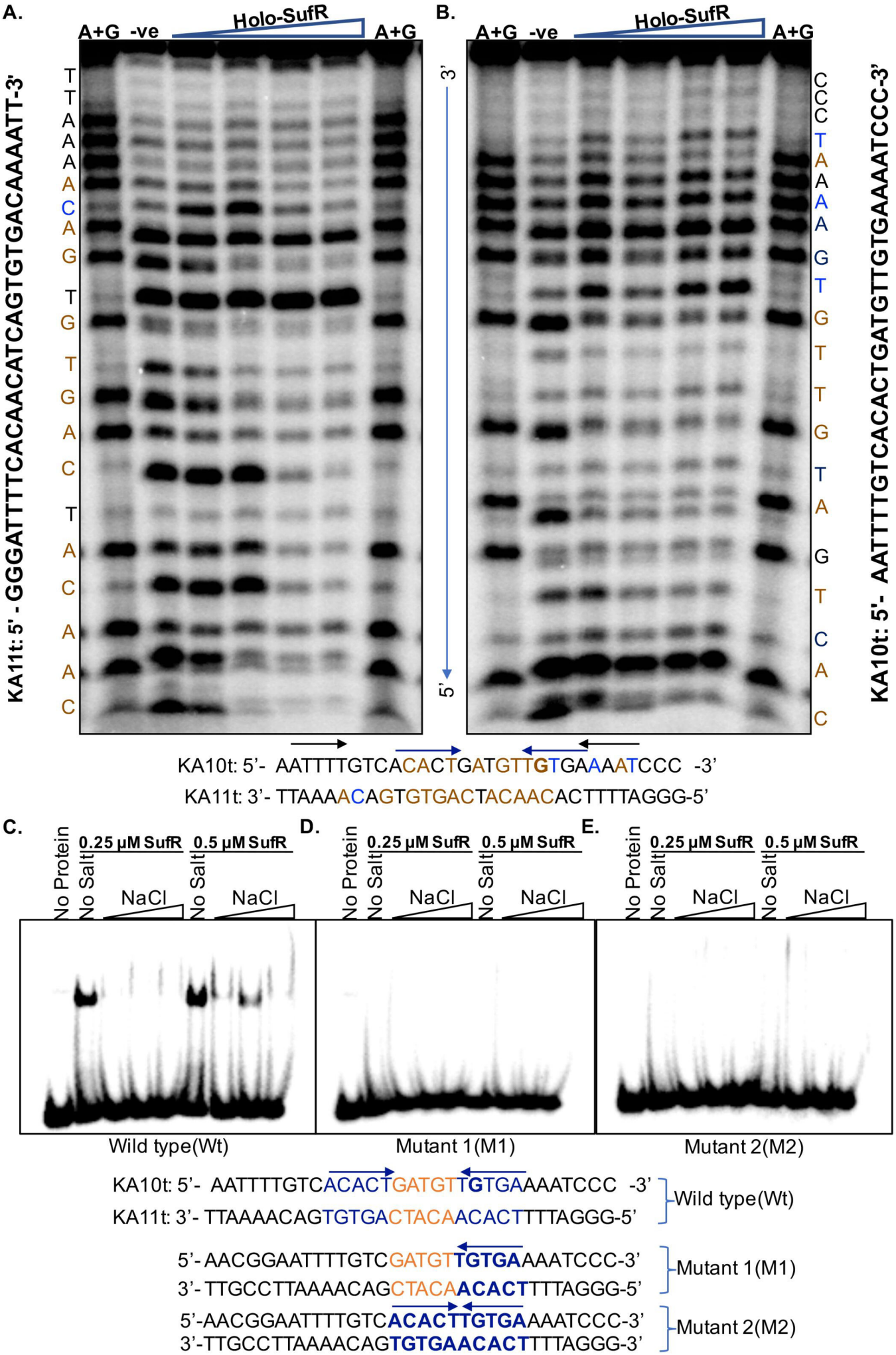
A.
A+G -ve
Holo-SufR
A+G
KA11t: 5' - GGGATTTTCACAACATCAGTGTGACAAAATT-3'
B.
A+G -ve
Holo-SufR
A+G
3'
5'
KA10t: 5' - AATTTTGTCACACTGATGTTGTGAAAATCCC-3'
KA10t: 5'- AATTTTGTCACACTGATGTTGTGAAAATCCC -3'
KA11t: 3'- TTAAAACAGTGTGACTACAACACTTTTAGGG-5'
C.
D.
E.
No Protein
No Salt
0.25 μM SufR
0.5 μM SufR
NaCl
Wild type(Wt)
Mutant 1(M1)
Mutant 2(M2)
KA10t: 5'- AATTTTGTCACACTGATGTTGTGAAAATCCC -3'
KA11t: 3'- TTAAAACAGTGTGACTACAACACTTTTAGGG-5'
Wild type(Wt)
5'- AACGGAATTTTGTCGATGTTGTGAAAATCCC-3'
3'- TTGCCTTAAAACAGCTACAACACTTTTAGGG-5'
Mutant 1(M1)
5'-AACGGAATTTTGTCACACTTGTGAAAATCCC-3'
3'-TTGCCTTAAAACAGTGTGAACACTTTTAGGG-3'
Mutant 2(M2)

Figure 10

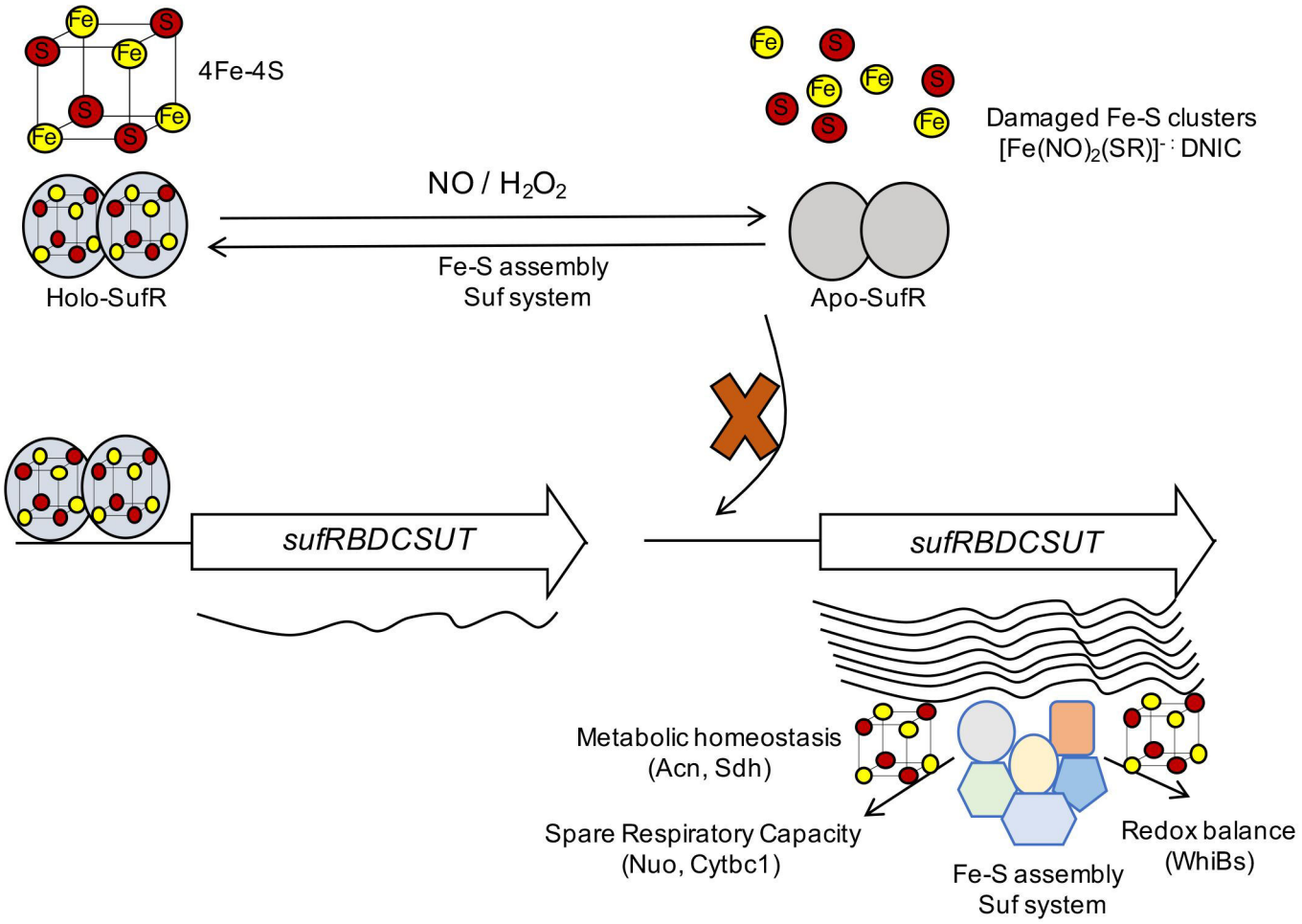

- **Stress tolerance**
- **Persistence**

Figure 1-figure supplement 1

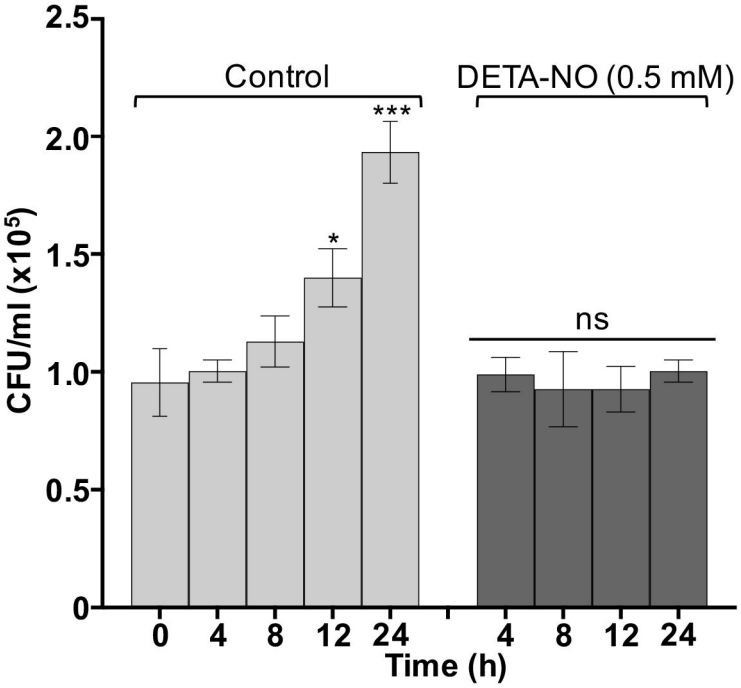

Figure 1-figure supplement 2

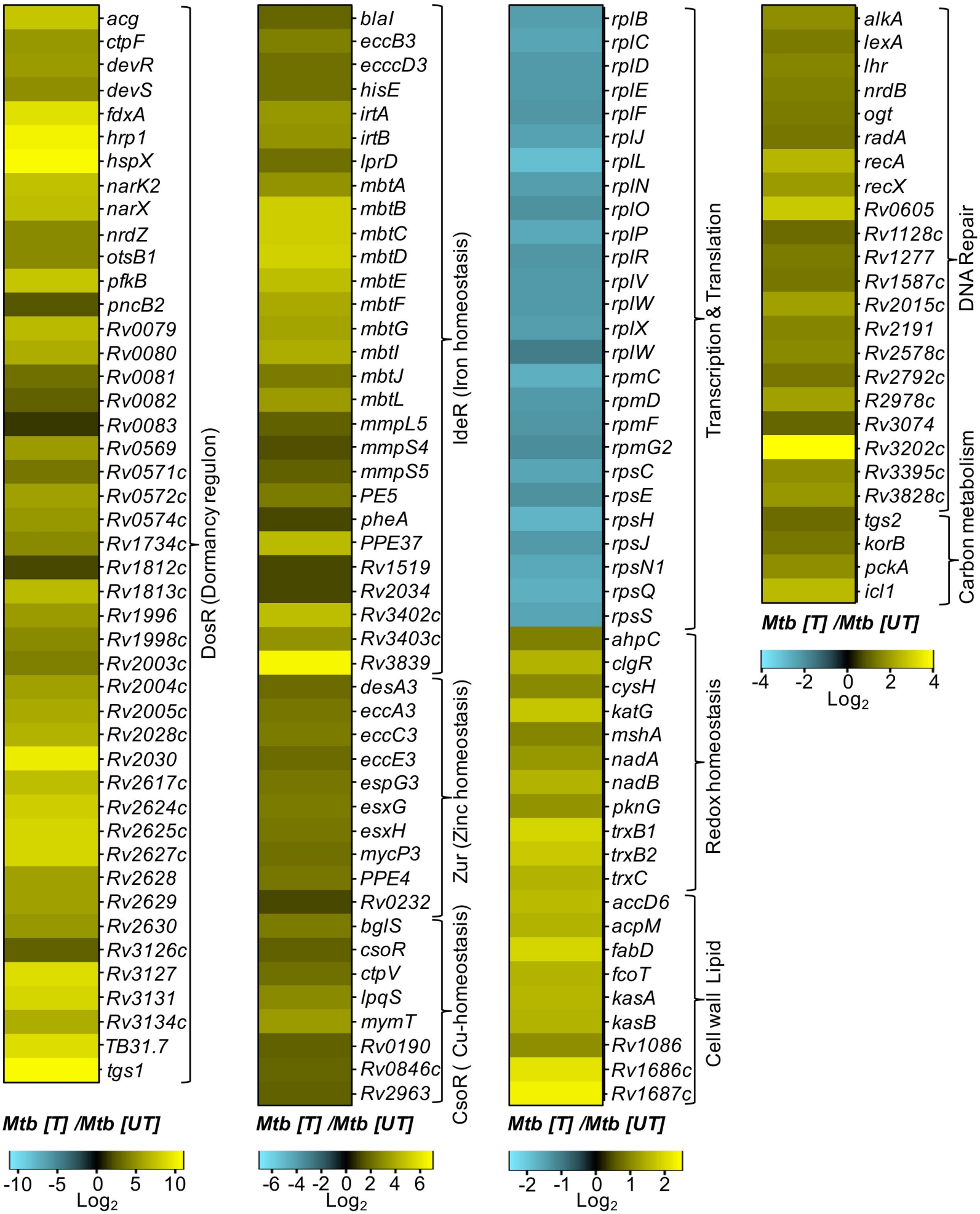

Figure 3-figure supplement 1

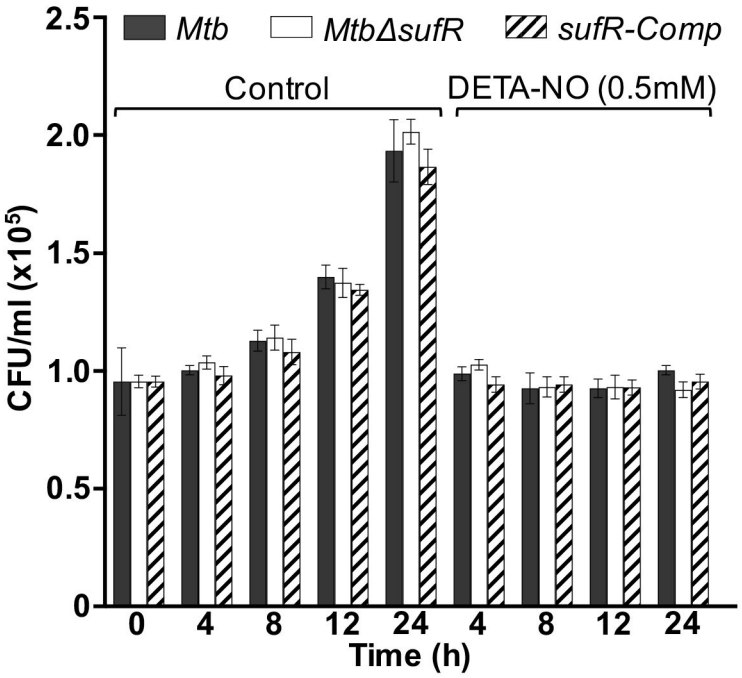

Figure 3-figure supplement 2

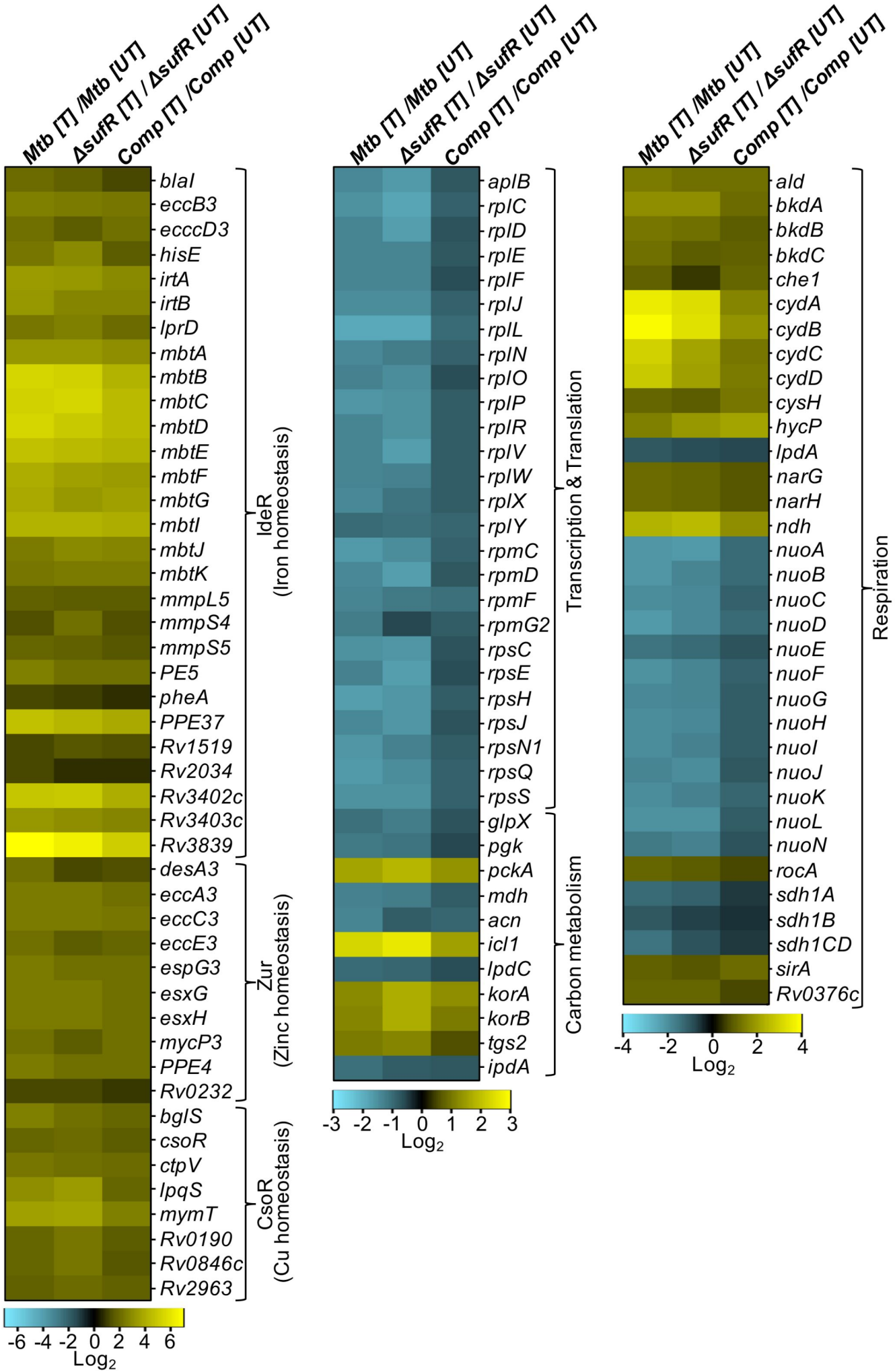

Figure 3-figure supplement 3

A.

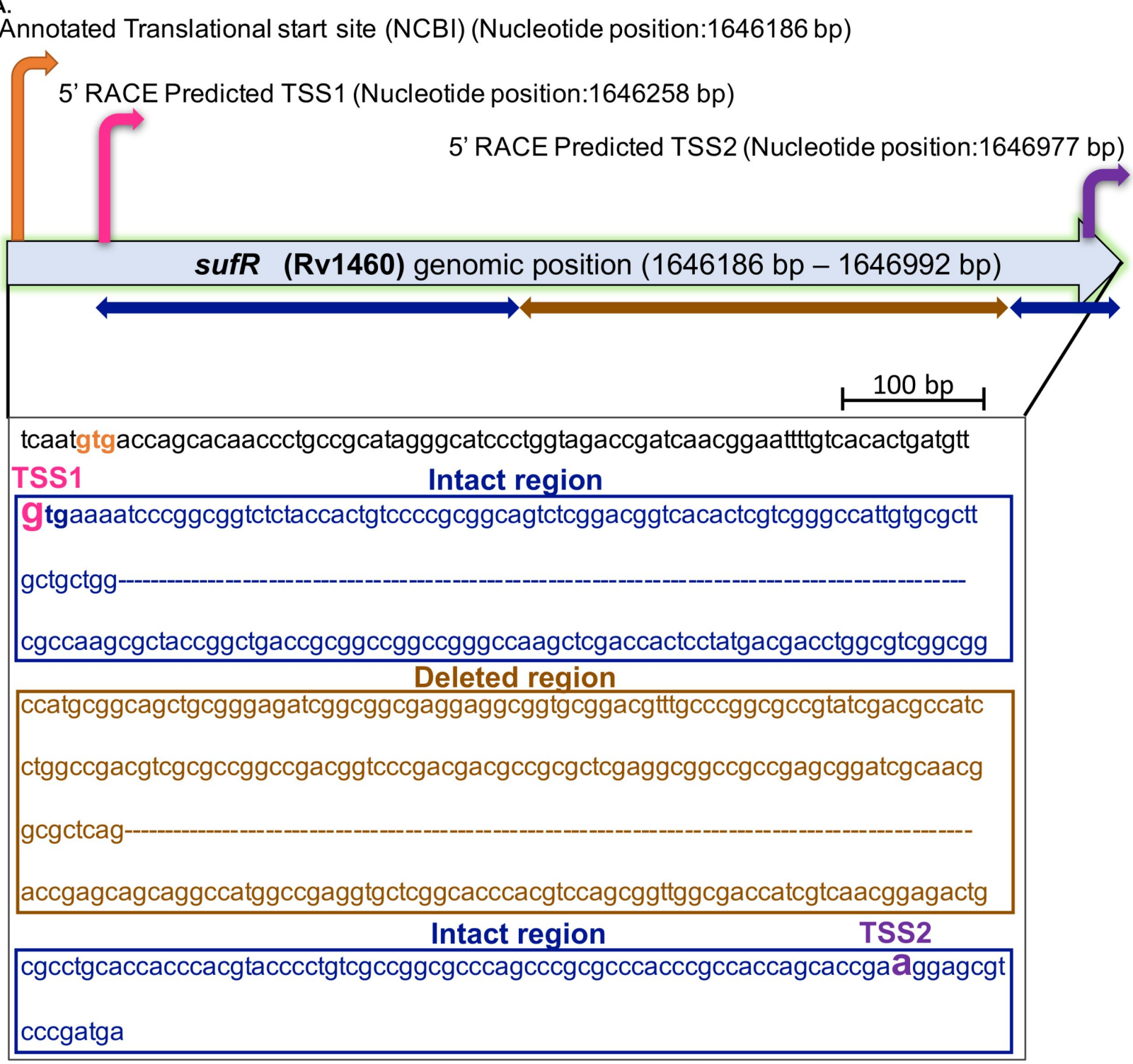

B.

Comparison	Log_2 fold change	FDR	Abs fold change	Regulation
***Mtb* [T] vs *Mtb* [UT]**	4.620428305	5.37E-18	24.59730422	Up
***Mtb ΔsufR* [T] vs *Mtb ΔsufR* [UT]**	1.672581636	7.89E-10	3.187845335	Up
***sufR-Comp* [T] vs *sufR-Comp* [UT]**	2.31000536	4.18E-13	4.958849223	Up
***Mtb ΔsufR* [UT] Vs *Mtb* [UT]**	**1.984276389**	**1.61E-08**	**3.9566416**	Up
***sufR-Comp* [UT] Vs *Mtb* [UT]**	2.537077208	1.73E-11	5.804119437	Up
***Mtb ΔsufR* [UT] Vs *sufR-Comp* [UT]**	-0.552800818	0.007575	1.466930803	Down

Figure 4-figure supplement 1

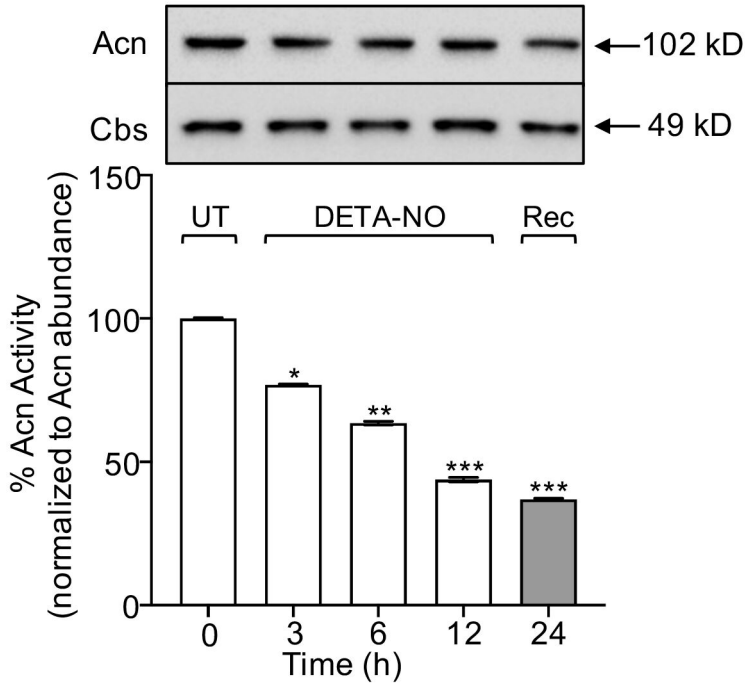

Figure 5-figure supplement 1

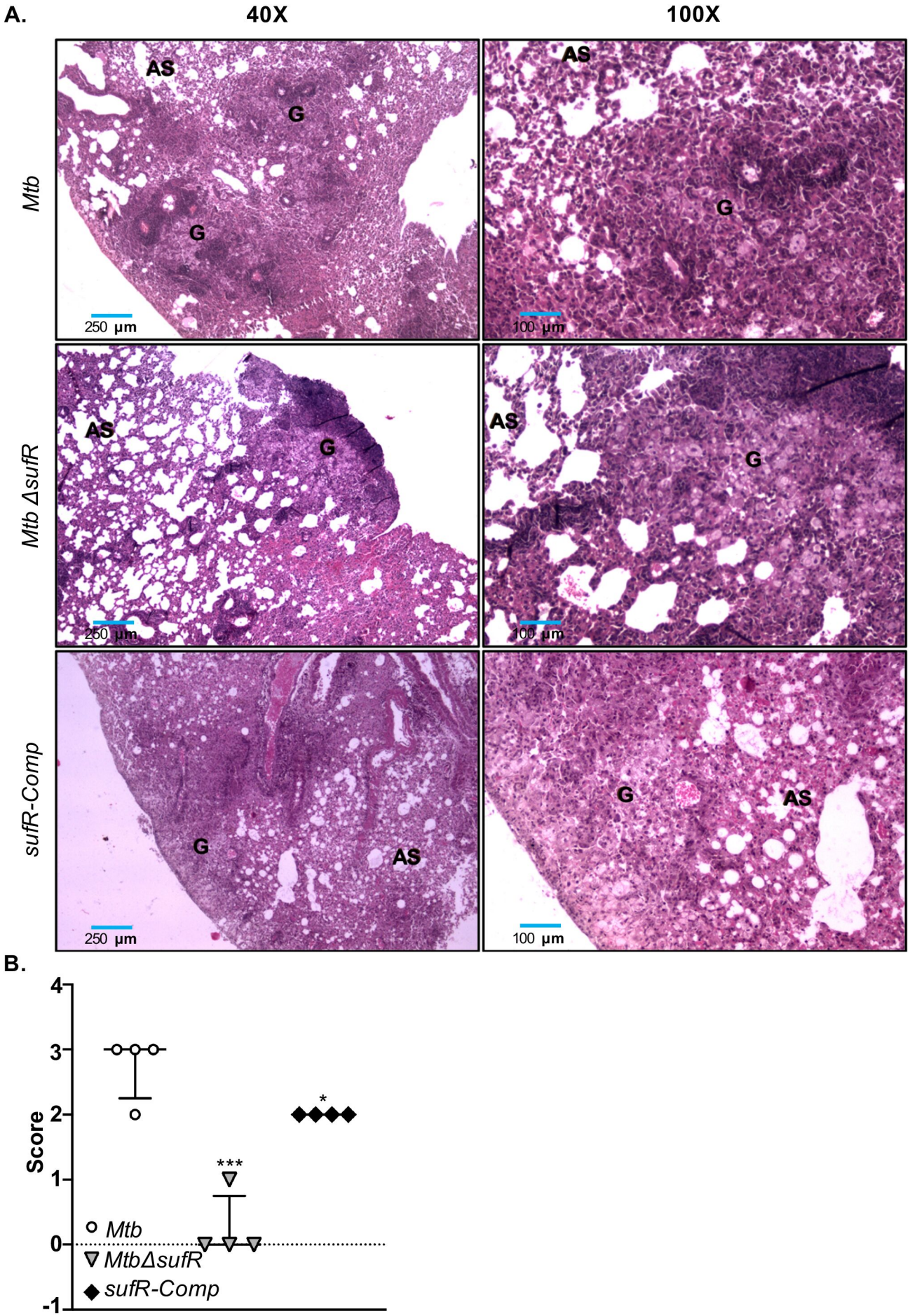

Figure 6-figure supplement 1

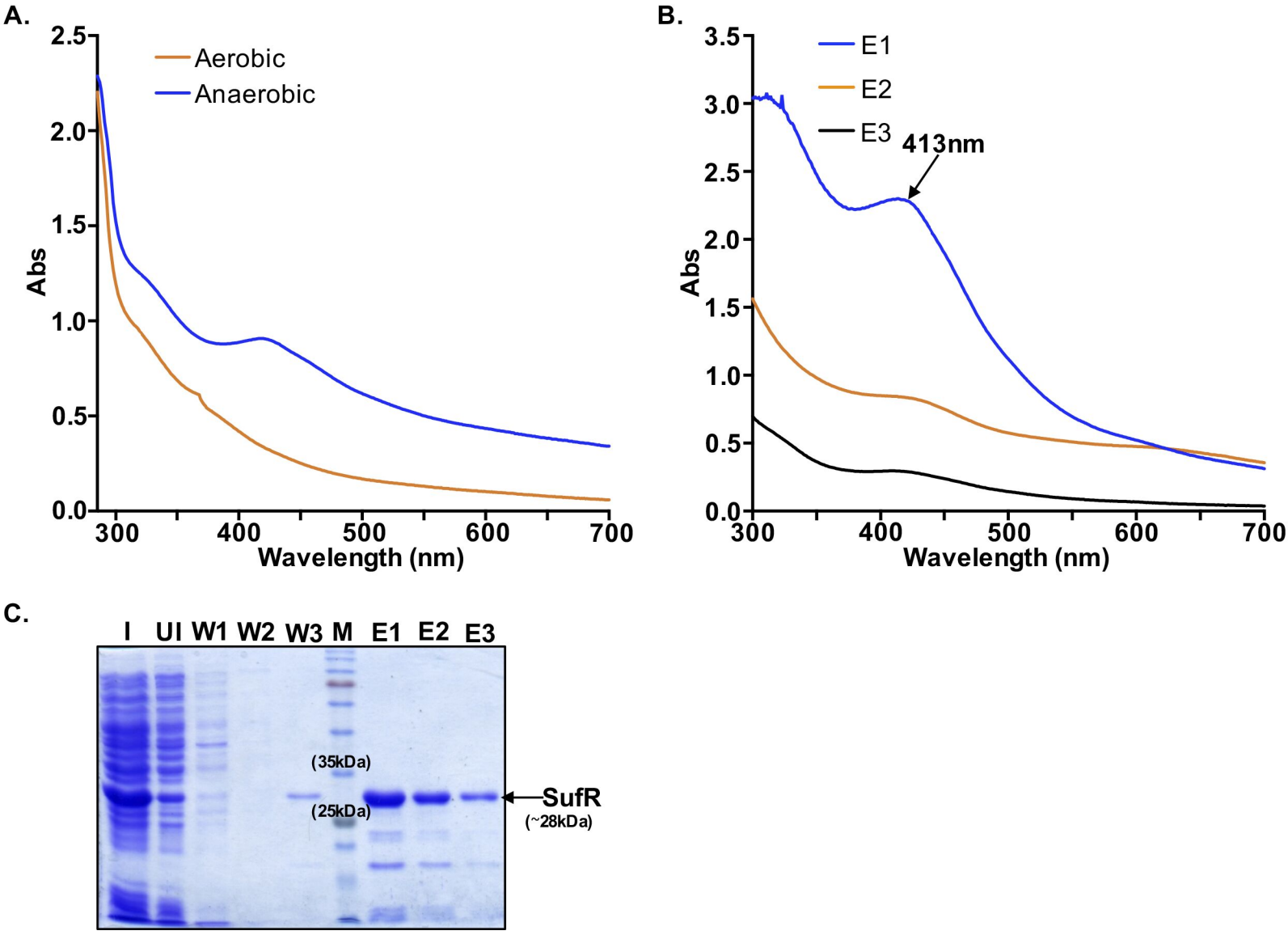

Figure 7-figure supplement 1

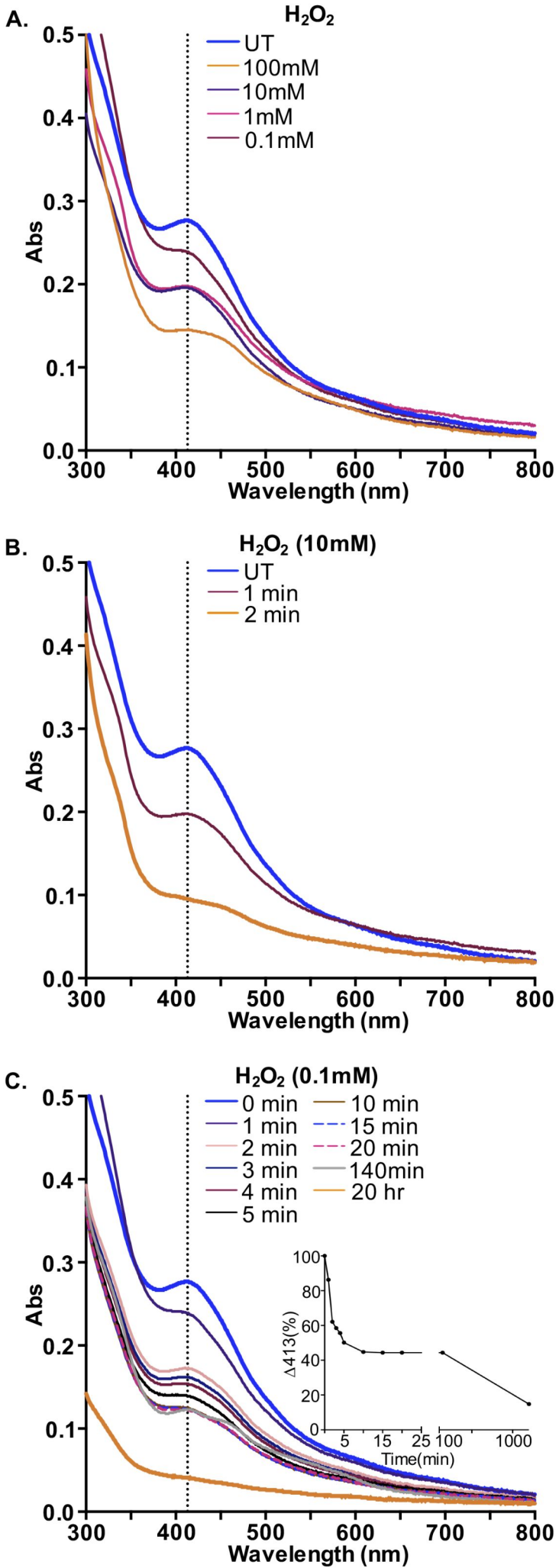
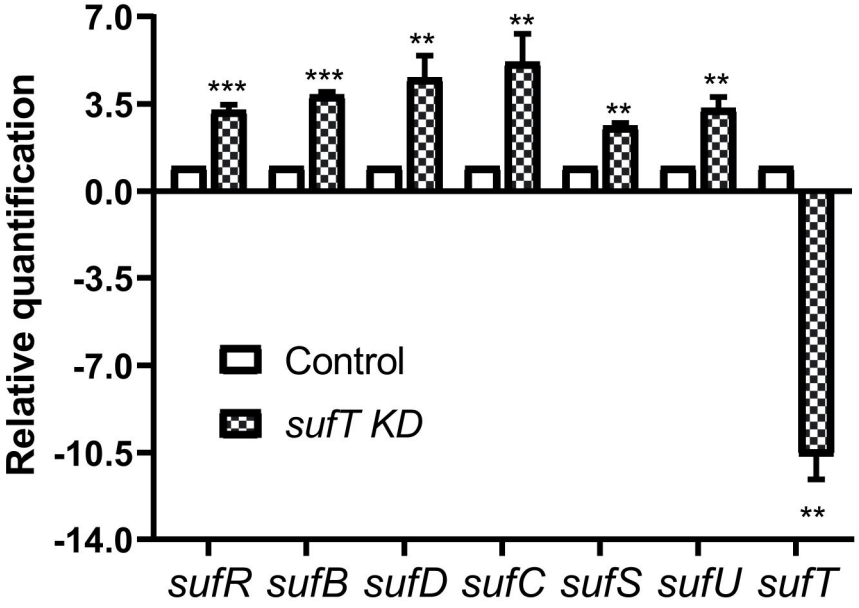
Figure 8-figure supplement 1